PERIODICO di MINERALOGIA
established in 1930

Dipartimento
di Scienze della Terra

Sapienza
Università di Roma

An International Journal of
Mineralogy, Crystallography, Geochemistry,
Ore Deposits, Petrology, Volcanology
and applied topics on Environment, Archaeometry and Cultural Heritage

Thermal metamorphism of the mantle peridotites from Paleozoic accretionary prism by Eocene pluton (NE of Anarak, Kal-e-Kafi area, Central Iran)

Zahraalsadat Zakipour [1], Ghodrat Torabi [1,*], Nakashima Kazuo [2], Tomoaki Morishita [3]

[1] Department of Geology, University of Isfahan, Azadi Square, 8174673441, Isfahan, Iran
[2] Department of Earth and Environmental Sciences, Yamagata University, Yamagata 990-8560, Japan
[3] School of Natural System, College of Science and Engineering, Kanazawa University, 920-1192 Kanazawa, Japan

ARTICLE INFO

Submitted: May 2022
Accepted: August 2022
Available on line: August 2022

* Corresponding author:
Torabighodrat@sci.ui.ac.ir

Doi: 10.13133/2239-1002/17755

How to cite this article:
Zakipour Z. et al. (2022)
Period. Mineral. 91, 163-199

ABSTRACT

The Eocene pluton intrudes the Paleozoic accretionary wedge in the Kal-e-Kafi area (NE of Anarak, Isfahan province, Central Iran). Metaperidotites of this Paleotethys- related accretionary prism consist of metalherzolite, metaharzburgite and metadunite and are associated with the listwaenites and metasediments (schist and marble).
Rock-forming minerals of the Kal-e-Kafi metaperidotites are olivine (forsterite and chrysolite, Mg# =0.86-0.92 with CaO<0.02 wt%), orthopyroxene (enstatite, Mg# =0.84-0.86), clinopyroxene (Mg# =0.90-0.94, Al_2O_3 0.03-2.08 wt%), tremolite, magnesio-hornblende, anthophyllite, serpentine, talc, chlorite, chromian spinel (Cr# =0.58-0.72), magnetite and plagioclase. All these minerals are metamorphic products and are not relicts of the primary igneous mineralogy, except the inner parts of Cr-spinels.
Chemical composition of the core of Cr-spinel crystals reveal that the protolith of the studied rocks were mantle peridotites which belong to the depleted and moderately depleted peridotite series.
The field relationships, petrography evidences, chemical characteristics of minerals and results of the thermobarometry calculations, show that the peridotites in the Kal-e-Kafi area have suffered a regional metamorphism in P-T condition of greenschist facies during the Paleozoic, intrusion of the Kal-e-Kafi pluton, caused a progressive contact metamorphism at 630 to 750 °C under a pressure less than 1 kbar (pyroxene hornfels facies) during the Eocene.

Keywords: Metaperidotite; Paleozoic; Kal-e-Kafi pluton; Eocene; Regional and contact metamorphism; Anarak; Central Iran.

INTRODUCTION

Ophiolite assemblages are relicts of the ancient oceanic crusts which are situated along the sutures (Coleman, 1977; Dilek and Newcomb, 2003). Petrological studies of these rock suits will be a great help in understanding the geological history of the area and pre, syn and post-obduction geological events affected the past oceanic lithosphere rocks. According to Coleman (1977), ophiolites are metamorphosed in two ways: (1) internal metamorphism, which includes events that affect the ophiolite minerals assemblage (e.g., serpentinization, as well as rodingite and liswaenite formation); and (2) external metamorphism which is related to the ophiolite emplacement, orogenic events and post-obduction metamorphism induced by either magma intrusion or regional metamorphism (e.g., Oliver et al., 1972; Paktunc, 1984; Dymek et al., 1988; Melcher et al., 2002; Torabi et al., 2011a; Khalili et al., 2016).

The ophiolites of Iran can be generally classified into two Paleozoic and Mesozoic age groups (Figure 1; Shafaii Moghadam and Stern, 2014). The ophiolites in north, northeastern of Iran and western part of the Central-East Iranian Microcontinent (CEIM; Yazd and Posht-e-Badam blocks) are remnants of the Paleozoic Paleo-Tethys oceanic crust (Torabi, 2011, 2012 a,b). On the other hand, the ophiolites situated along the Zagros thrust zone and around of the CEIM (Figure 1) are remnants of the Neo-Tethys oceanic crust and belong to the Mesozoic (Torabi et al., 2011b).

The Paleozoic age Jandaq, Anarak, Bayazeh and Posht-e-Badam ophiolites (Figure 2) are metamorphosed under P-T conditions of the upper amphibolite (Torabi et al., 2011b), greenschist and blueschist (Torabi, 2011, 2013), lower amphibolite (Khalili et al., 2016), and upper greenschist to lower amphibolite facies (Nosouhian et al., 2019), respectively.

The mantle peridotites of the Naein, Piranshahr and Deh-Salm Mesozoic ophiolites, have been metamorphosed under amphibolite (Shirdashtzadeh et al., 2014) and lower-amphibolite (Hajialioghli and Moazzen, 2014), respectively.

In the northeast of the Anarak city (Isfahan Province, Central Iran), the metamperidotites and listwaenites are associated with the Paleozoic schist and marble unit. These Paleozoic rocks are in contact with the Kal-e-Kafi Eocene pluton (Figure 3). The Kal-e-Kafi Paleozoic unite are considered to be a remnant of a Permo-Triassic accretionary prism (Bagheri, 2007; Bagheri and Stampfli, 2008) however, yet, no petrological study has been reported on these peridotites. In this contribution, we provide petrological studies on these metaperidotites to provide information regarding the geological evolution of this area. Moreover, we study the effects of the Kal-e-Kafi Eocene pluton on the peridotite unit.

In this research, we used the results of the field study, petrography evidences and chemical affinities of minerals to determine the conditions of this contact metamorphism.

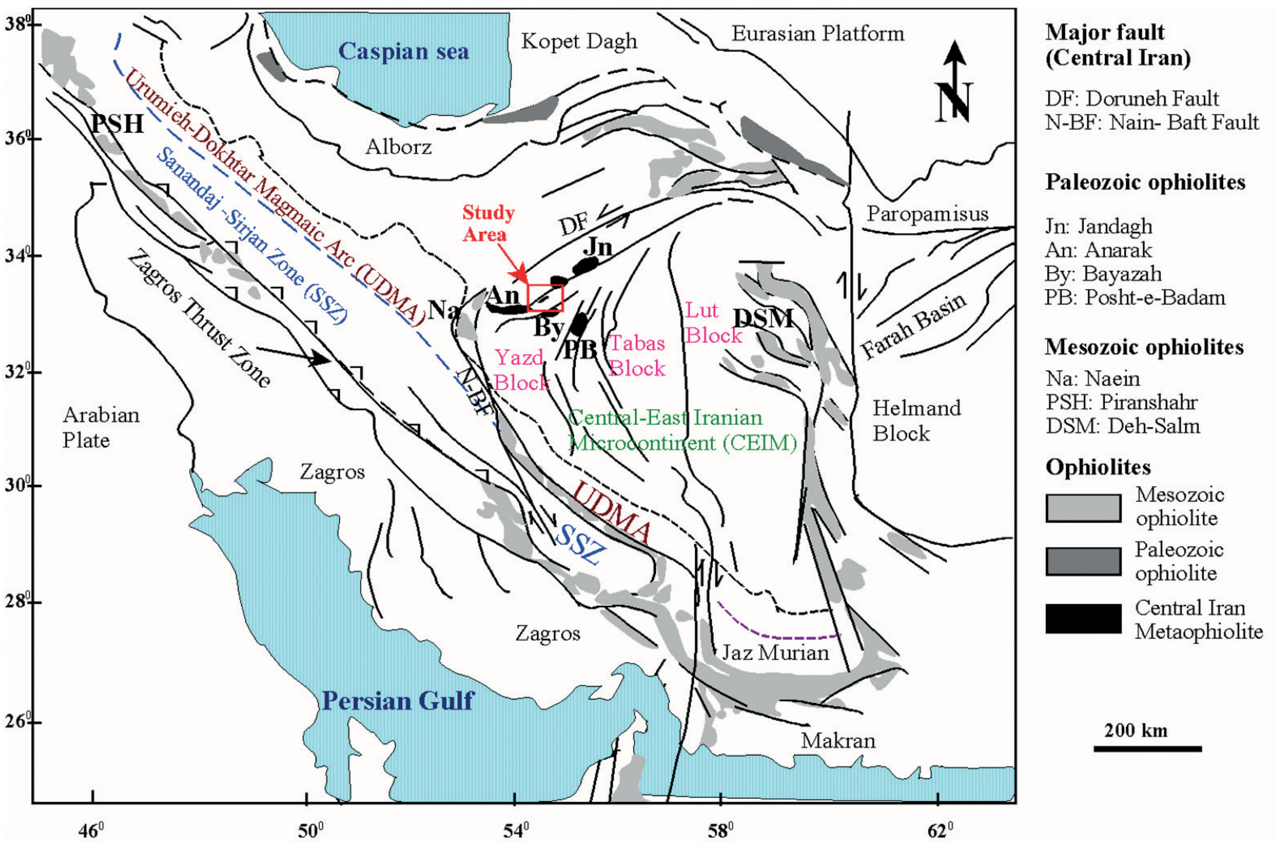

Figure 1. The main structural units of Iran and location of ophiolites and Kal-e-Kafi area (Stocklin, 1968; Bagheri, 2007; Zanchi et al., 2009, slightly modified).

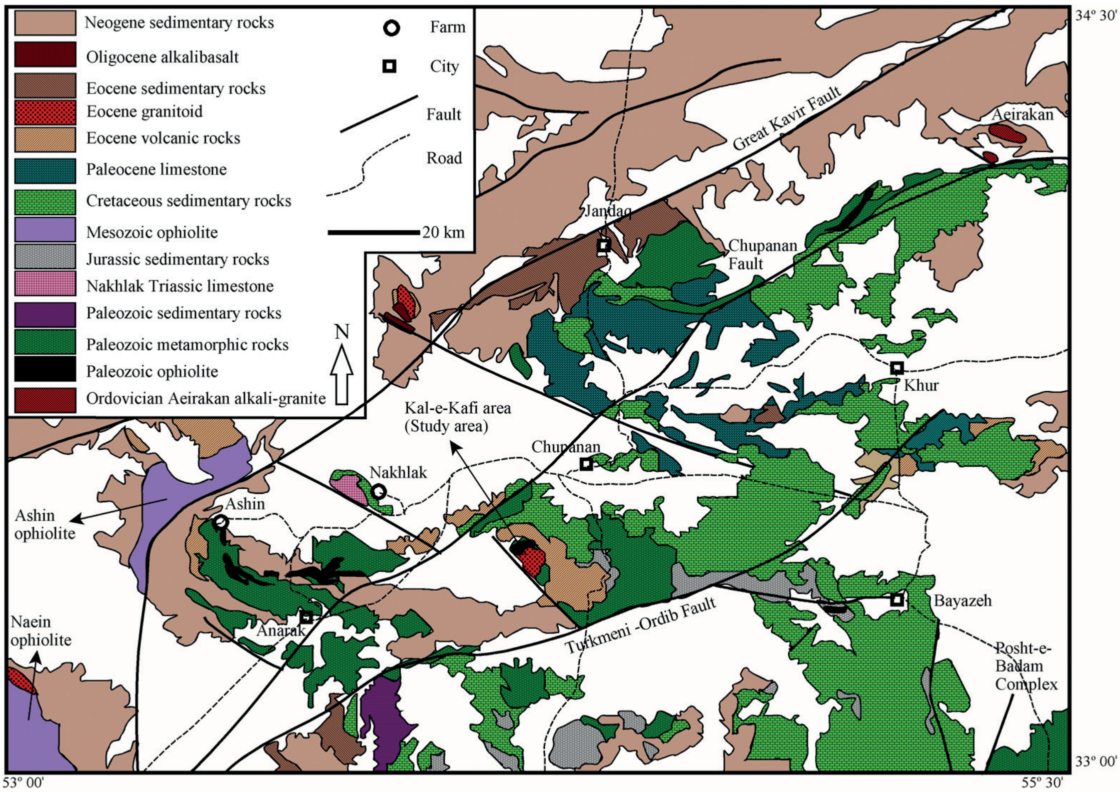

Figure 2. Simplified geological map of the Anarak-Khur area (Yazd Block, Central Iran; Aistov et al., 1984; slightly modified), and location of the study area.

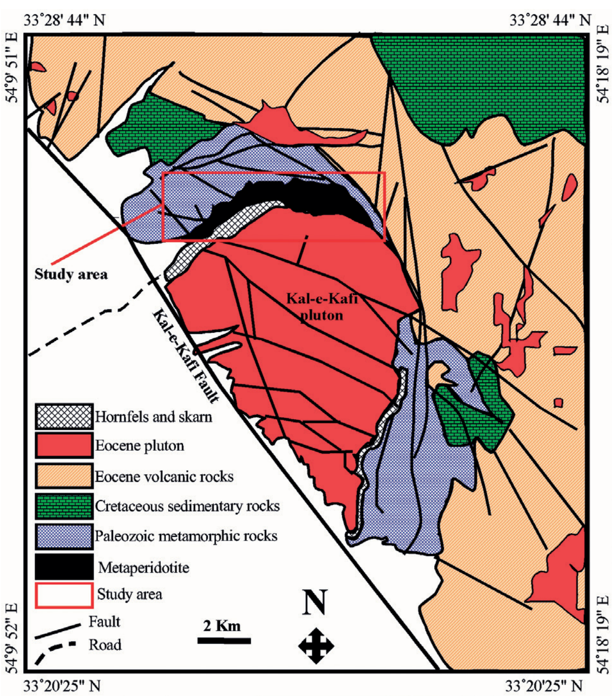

Figure 3. Simplified geological map of the Kal-e-Kafi area, northeast of Isfahan Province, Central Iran, based on 1:100000 scale map of Kabudan (sheet 6856), after Sharkovski et al. (1984).

REGIONAL GEOLOGY

The main structural units of Iran are: Folded Zagros, Zagros Thrust Zone (ZTZ), Urumieh-Dokhtar magmatic arc (UDMA), Central-East Iranian Microcontinent (CEIM), Sanandaj-Sirjan Zone (SSZ), Alborz, Kopet Dagh, Eastern Iran, and Makran (Stocklin, 1968; Bagheri, 2007; Zanchi et al., 2009; Figure 1). The CEIM is located between the convergent Arabian and Eurasian plates. This microcontinent was affected by a complex system of active intracontinental strikeslip faults that has divided this microplate into four main crustal domains, including: the Lut block, the Tabas (Kerman) block, the Posht-e-Badam block and the Yazd (Naein) block, from the east to the west, respectively (Figure 1). Several ophiolitic belts are present in and around of the CEIM that are remnants of the Paleo- Tethys and Neo-Tethys oceanic crusts.

The Kal-e-Kafi area is situated in the western part of the CEIM (Northwestern part of the Yazd) block (Figure 1).

Deep faults of the this area are often the location of ophiolitic bodies exposure (Romanko et al., 1984). Geological studies of the Kal-e-Kafi area indicate that the lowermost rock units of the area are the Paleozoic metaperidotites and liswaenites which are covered by Paleozoic metasediments (schist and marble) (Torabi, 2013; Figure 4). The Anarak area ophiolite and metamorphic rocks have passed the greenschist metamorphism condition (Torabi, 2013). There are no chromitite in the Anarak area ophiolite (Torabi, 2012b). $^{40}Ar/^{39}Ar$ isotopic analyses of these metamorphic rocks indicate the ages of 319.0 and 333.9 Ma (Carboniferous age; Bagheri and Stampfli, 2008). The Cretaceous limestones overlie the Paleozoic metamorphic rocks with erosional angular unconformity (Nazari et al., 2019). The Cenozoic rock units of the area are Eocene volcanic and intrusive bodies, skarn and hornfels (Figure 3).

This Eocene pluton cuts all the rock units in the area from Paleozoic to Eocene (Nazari et al., 2019). The Kal-e-Kafi pluton presents a wide range of composition from gabbro to anorthosite, diorite, monzonite and granite (Salim, 2019; Salim et al., 2018). Intrusion of the Eocene magma into metaperidotites in northern part of the area, caused contact metamorphism. The skarn and hornfels are formed by contact metamorphism between the Kal-e-Kafi pluton and Paleozoic marble and schist, respectively (Ranjbar et al., 2016). The hornfels and skarn were formed by thermal metamorphism occurrence in the P-T condition of hornblende hornfels and pyroxene hornfels facies.

The K-Ar dating of the study area Eocene volcanic rocks yield 53 and 48 Ma (Yakovenko et al., 1981; Aistov et al., 1984). The U-Pb dating of zircons from the Kal-e-Kafi pluton yield the Early Eocene ages of 50.3 and 52±1 Ma (Ahmadian et al., 2016). The younger phase of this pluton formed the Kal-e-Kafi porphyry Cu-Mo-Au deposit (Mahdavi et al., 2015; Ahmadian et al., 2016).

The lower Oligocene lamprophyric dykes and stocks, intruded into the Eocene volcanic rocks of the area, which are exposed in the east of the Kal-e-Kafi area (Nazari et al., 2019).

METHODS OF STUDY

Chemical analyses of minerals from 10 metaperidotite samples were conducted by wave-length-dispersive electron probe microanalyzer (EPMA) using a JEOL JXA-8800R, JEOL JXA-8600 at the Earth Science Department of Kanazawa University (Kanazawa, Japan) and Department of Earth and Environmental Sciences of Yamagata University (Yamagata, Japan), respectively. These analyses were performed with an accelerating voltage of 20 kV, a beam current of 20 nA with 3-μm probe beam diameter, detection limits of 0.05 wt%, and a maximum 40-s counting interval. Representative chemical analyses of the minerals and their calculated structural formula are shown in Tables 1 to 9.

XRD analyses of the metaperidotite samples were carried out by Bruker D8 Advance X-ray diffractometer at the Central Laboratory of the University of Isfahan. The trace element contents of clinopyroxenes from the Kal-e-Kafi metaperidotites were obtained by laser ablation ICP-MS (LA-ICP-MS) using an ArF 193 nm Excimer Laser coupled to an Agilent 7500S at the Earth Science Department of the Kanazawa University (Japan) (Table 10).

The amounts of Fe^{3+} and Fe^{2+} in minerals were estimated by assuming mineral stoichiometry. All the metamorphic reactions presented in this article are from Spear (1995). Minpet 2.02 software was used to plot minerals chemical composition in diagrams. The Cr#, Mg# and Fe# of minerals are calculated as Cr/(Cr+Al), $Mg/(Mg+Fe^{2+})$ and $Fe^{2+}/(Fe^{2+}+Mg)$ atomic ratio of minerals, respectively. Mineral names abbreviations are from Whitney and Evans (2010).

PETROGRAPHY

Metaperidotites of the Kal-e-Kafi area are grayish-green to dark-green in color and in the hand specimen.

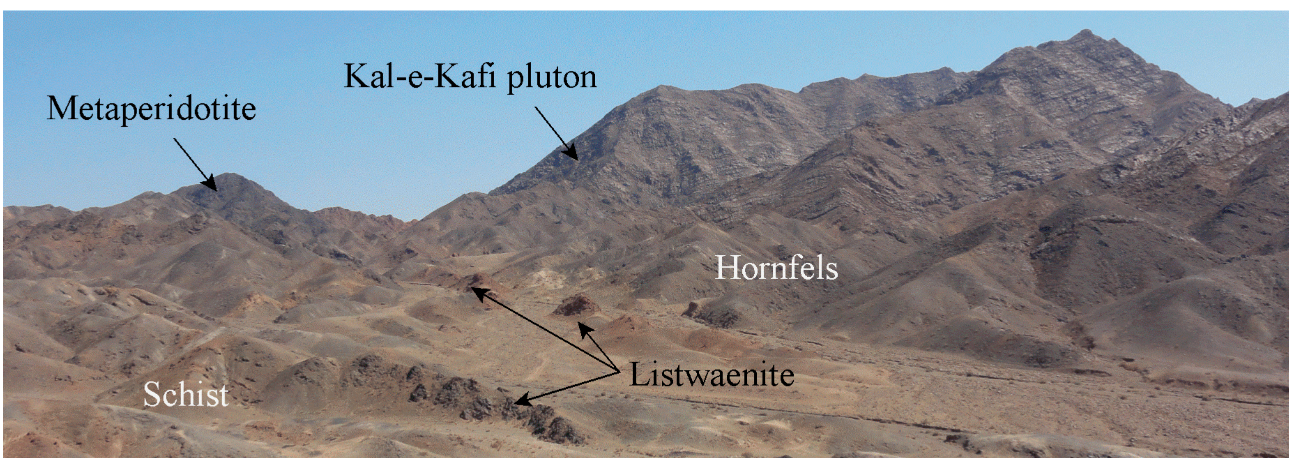

Figure 4. Field photographs of the studied metaperidotites, granitoid intrusive body of the Kal-e-Kafi and Paleozoic schist and marble.

These rocks do not show clear lineation and foliation. According to the petrography and mineral assemblages, the metaperidotites of this area comprise three principal rock types that are include metalherzolite, metaharzburgite and metadunite (Figure 5).

Metalherzolites are characterized by the presence of high amounts of tremolite and chlorite. Metaharzburgites are rich in talc, anthophyllite and enstatite. Metadunites are in contact with the Eocene pluton and are characterized by olivine and serpentine mineralogy. Petrography study of these metaperidotites indicates that granoblastic, porphyroblastic, nematoblastic and poikiloblastic are the main textures and Jack-straw texture is restricted to the tremolite-bearing metalherzolites.

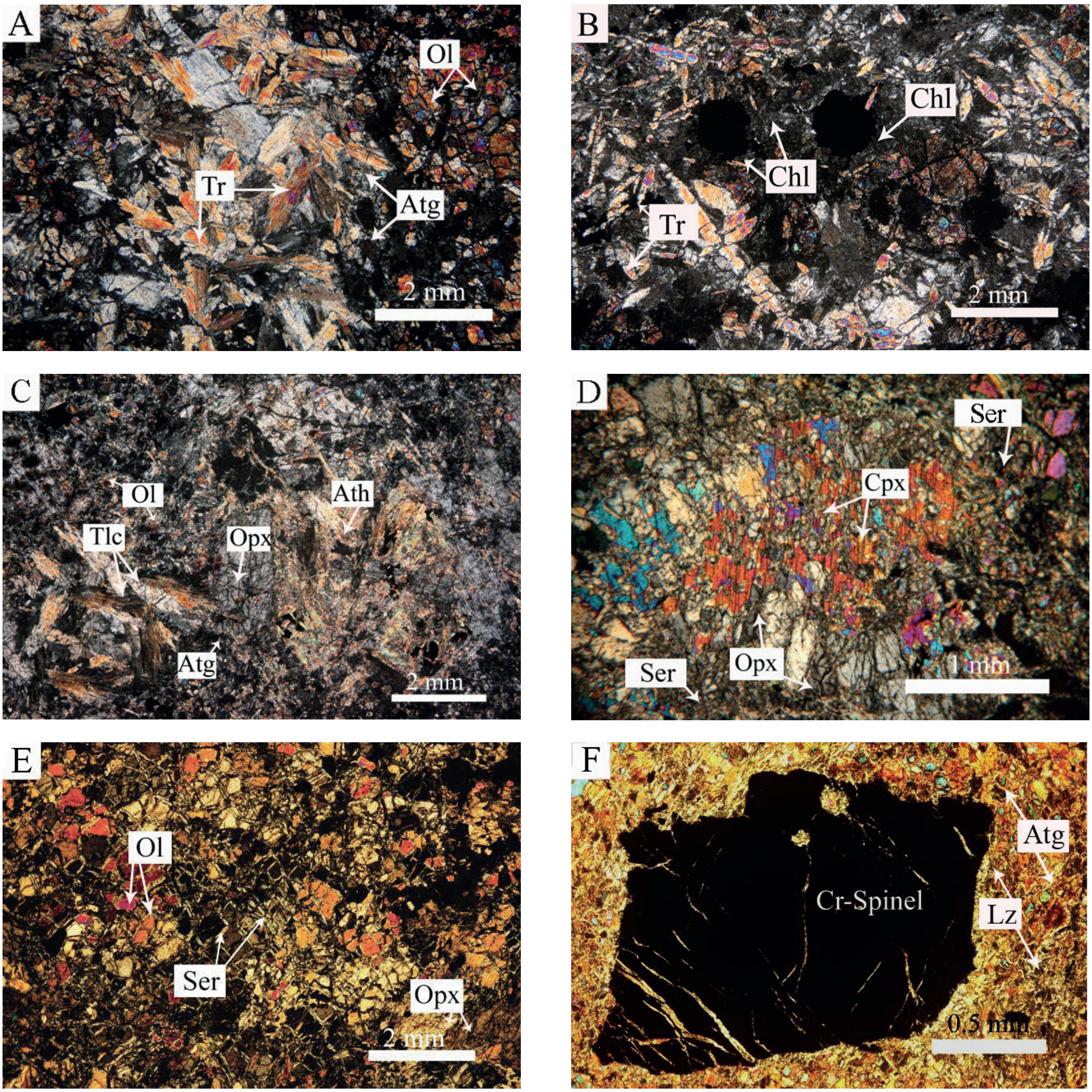

Figure 5. Photomicrographs (in crossed-polarized light) of (A) Olivine neoblasts associated with tremolite and, (B) Formation of chlorite around Cr-Magnetite in the metalherzolites. (C) Formation of orthopyroxene at the expense of talc and olivine and, (D) Clinopyroxene associated with orthopyroxene and serpentine in the metaharzburgites. (E) Olivine neoblasts and mesh texture containing serpentine and, (F) Subhedral Cr-spinel grain in the metadunites.

Metalherzolite

Rock-forming minerals of metalherzolites are olivine, tremolite, serpentine, clinopyroxene, chromian magnetite, magnetite and chlorite. The studied metalherzolites exhibit the porphyroblastic, granoblastic, nematoblastic, poikiloblastic, jack-straw and mesh textures.

Olivine neoblasts are in equilibrium with the pyroxene minerals (Figure 5A). There are magnetite inclusions in olivines.

Some of the olivines are altered to serpentine minerals (Figure 5A). X-ray diffraction (XRD) pattern shows that the main serpentine minerals of metalherzolites are of antigorite type (Figure 6). Antigorites are associated with the chlorites.

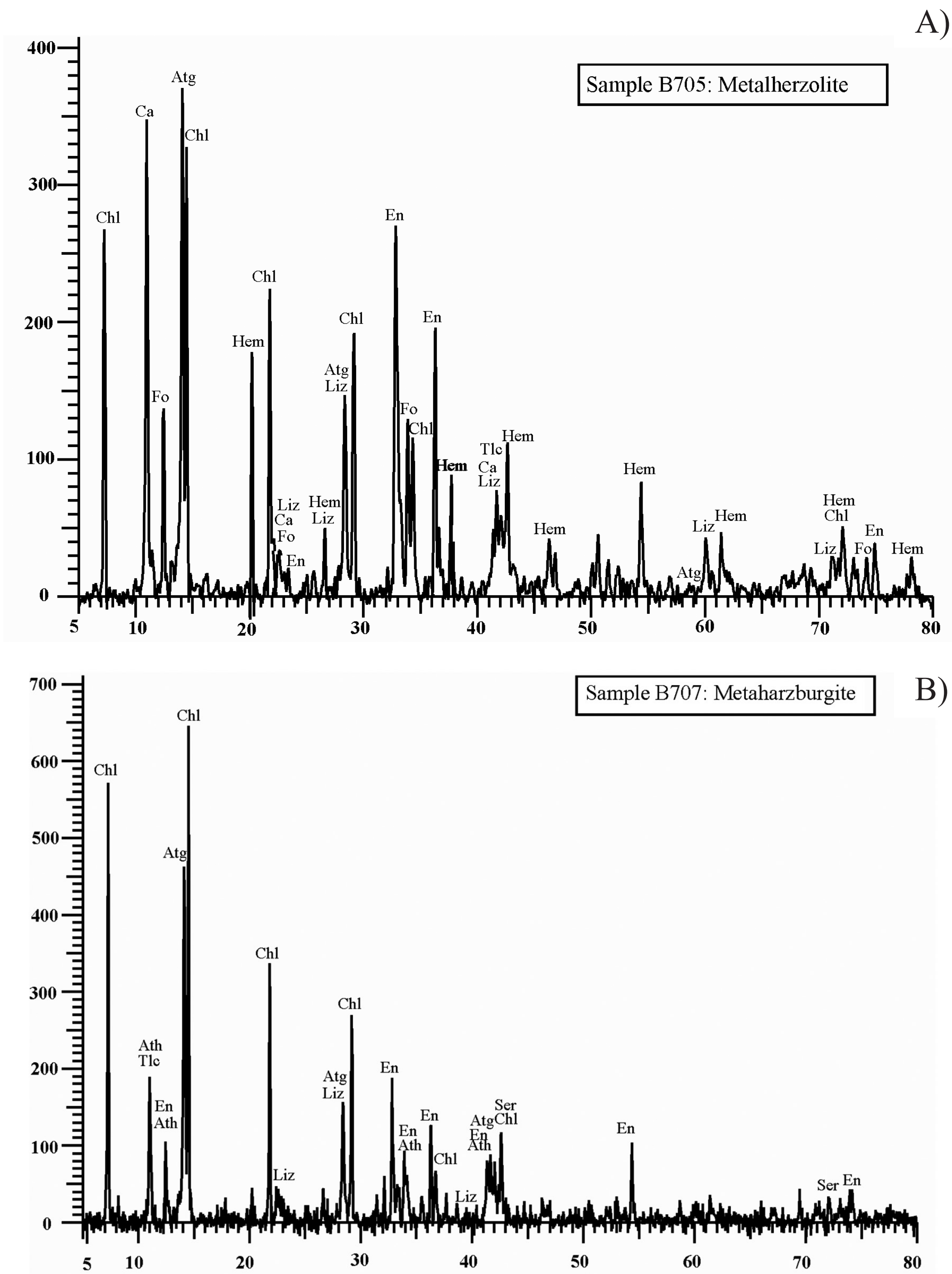

Figure 6. X-ray diffraction patterns of the metalherzolite and metharzburgite samples from the Kal-e-Kafi area.

Tremolite is the most important Ca-bearing silicate in the metalherzolites, but small amount of clinopyroxene is also present (Figure 5A).

Chromian spinels are relicts of the primary igneous mineralogy. They are the most resistant minerals against the metamorphism and alteration. Primary chromian spinel is accessory mineral of these metaperidotites. This mineral is anhedral to subhedral in morphology. The modal abundance of spinels in all samples are less than 3 vol% and partly are altered to magnetite and chromian magnetite, but in some rock samples their internal parts remain intact.

Chlorites exhibit a faintly green pleochroismus. They are common in the matrix and sometimes in veinlets. These minerals are often associated with tremolite and magnetite spinel and in form of accumulations with serpentines (Figure 5B). Chlorite content of the metalherzolites is higher than the metaharzburgites.

Metaharzburgite

These rocks are composed of olivine, orthopyroxene, talc, anthophyllite, serpentine, magnetite, Cr-spinel, ± low amounts of clinopyroxene, chlorite and tremolite. Near to the Kal-e-Kafi Eocene pluton, minor amount of plagioclase (<2 vol%) is also present in the metaharzburgites. Main textures of metaharzburgites are porphyroblastic, granoblastic, poikiloblastic, nematoblastic and mesh texture.

Olivine grains in the metaharzburgites present slightly higher modal abundance than in the metalherzolites and more serpentinization.

Orthopyroxene makes the poikiloblastic and porphyroblastic textures, and found with talc, olivine and anthophyllite (Figure 5C). Some orthopyroxene porphyroblasts partially replaced by serpentine in margin that indicates a retrograde metamorphism occurrence (M3) after formation of metamorphic orthopyroxenes (M2).

Talc is a common product of metamorphism in the metaharzburgites. It is formed along the cleavages and cracks of some minerals, such as orthopyroxene and olivine (Figure 5C).

Anthophyllite can be identified by its parallel extinction and lack of twinning. This mineral makes sheaf-like aggregates and fills the cracks (Figure 5C).

Low amounts of clinopyroxene observed in the metaharzburgite (less than 2 vol%). Clinopyroxenes are fine grained and anhedral in morphology (Figure 5D). They are associated with orthopyroxene and serpentine and possibly have metamorphic nature.

Most of the Cr-spinels in the metaharzburgites are completely changed into the magnetite and chromian magnetite (Figure 5B), but in some cases they have fresh core.

Plagioclases of the metaharzburgites which are in contact with the Eocene pluton, are generally small in size and anhedral to subhedral in morphology.

X-ray diffraction analysis (XRD patterns) of serpentine minerals in the metaharzburgites shows that serpentines are mostly antigorite which caused to development of the mesh-texture in these rocks (Figure 5D).

Metadunite

Metadunites present lesser outcrops than the other types of metaperidotites in the Kal-e-Kafi area. They are found in contact with the Eocene pluton. Metadunites have yellow-green colour in hand specimen and present higher degrees of serpentinization than metaharzburgite and metalherzolite. The main texture of metadunites is granoblastic, but serpentinization process makes the mesh texture.

The main minerals are olivine and serpentine and the minor minerals are orthopyroxene, clinopyroxene and spinel (Figure 5E). Olivines are euhedral and larger than that in metaharzburgite and metalherzolite. Chromian spinels are euhedral to subhedral in morphology and occur as disseminated grains (Figure 5F). Some of the Cr-spinel grains are altered to chromian magnetite and magnetite.

Olivine grains are highly dissected by network serpentine veins, forming interlocking or equigranular texture. Antigorite and lizardite are the main varieties of serpentine that are present in metadunites (Figure 5F), but antigorite is the predominant serpentine mineral.

MINERAL CHEMISTRY

Olivine

Chemical composition of olivines in the studied metaperidotites shows that olivines are rich in Mg and are forsterite and chrysolite in composition (Figure 7A; Deer et al., 1992). The forsterite content of olivines varies from 86 to 91% in metalherzolites, 87 to 91% in metaharzburgites and 90 to 91% in metadunites (Table 1).

Olivines in the studied metaperidotites have very low content of CaO (<0.02 wt%). FeO* and MnO contents of olivines are 8.78 to 13.33 and 0.16 to 0.36 wt% in metalherzolites, 8.98 to 12.44 and 0.06 to 0.30 wt% in metaharzburgites and 7.90 to 10.04 and 0.14 to 0.24 wt% in metadunites, respectively (Table 1).

Orthopyroxene

Othopyroxenes in the studied metaperidotites, have enstatite composition (Figure 7B) in the classification diagram of pyroxenes (Deer et al., 1992). Enstatite amount varies from 86.10 to 87.27% in metalherzolites, 83.63 to 91.05% in metaharzburgite and 90.1 to 91.10% in metadunites, respectively. The Mg# content of

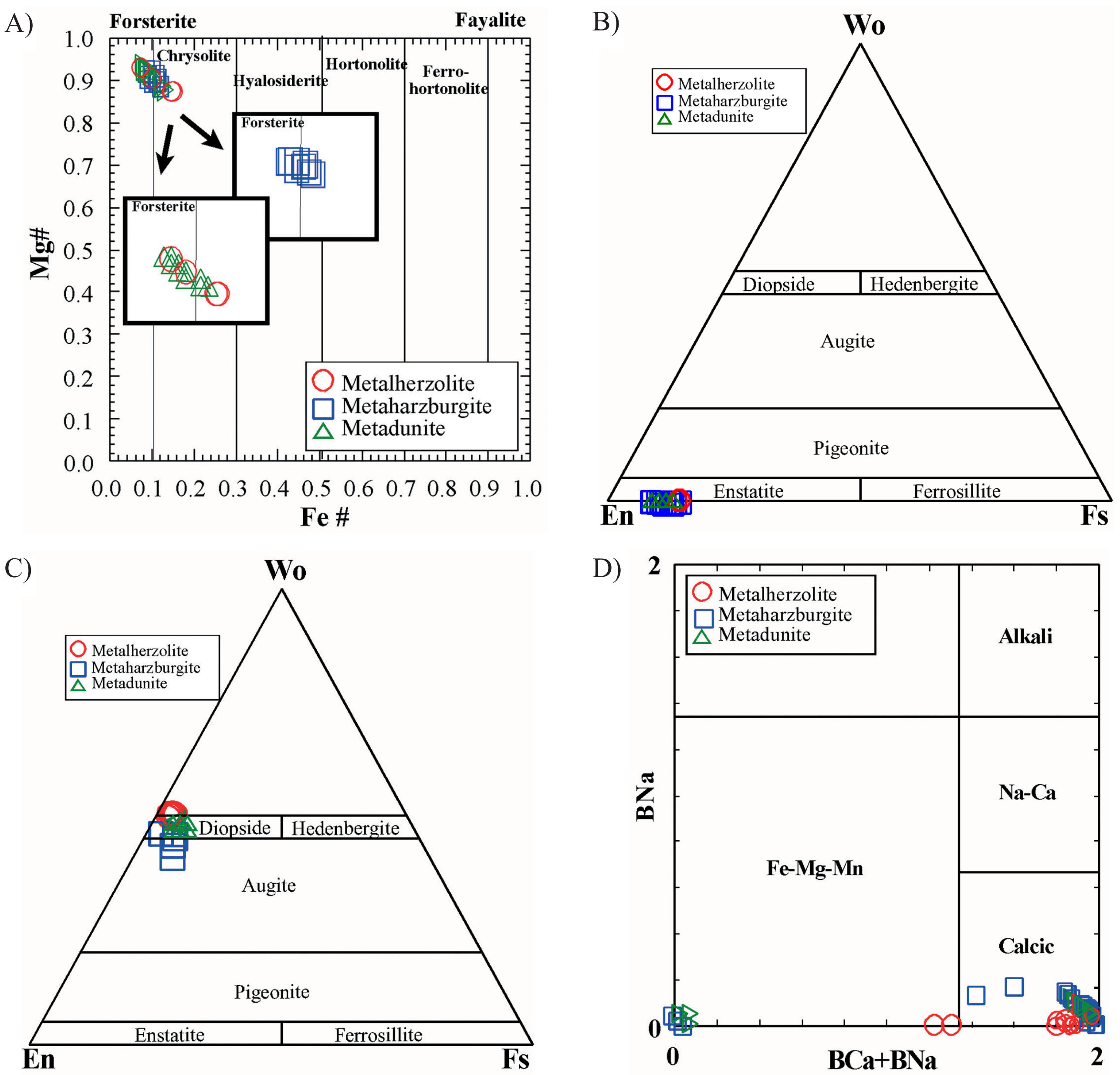

Figure 7. (A) The classification diagram of olivines (Deer et al., 1992); (B) Wo–En–Fs graph of orthopyroxenes from Deer et al. (1992); (C) Wo-En-Fs graph of clinopyroxenes from Deer et al. (1992). (D) Chemical classification graph of amphiboles into four principle groups (Leake et al., 1997); . The chlorites from the Kal-e-Kafi metaperidotites are clinochlore in composition.

othopyroxenes in metalherzolites, metaharzburgites and metadunites are calculated as 0.87 to 0.88, 0.86 to 0.91 and 0.83 to 0.86, respectively (Table 2).

Clinopyroxene

Clinopyroxenes of the studied metaperidotites have low contents of TiO_2 (0-0.12 wt%), Al_2O_3 (0.03-2.08 wt%), Na_2O (0-0.32 wt%) and Cr_2O_3 (0-0.06 wt%). Mg# values of these clinopyroxenes vary from 0.93 to 0.99 wt% (Table 3). Mineral chemistry of the analyzed clinopyroxenes shows that these minerals are diopside in composition (Figure 7C).

Amphiboles

Amphiboles in the studied metaperidotites can be classified into calcic and magnesian (Figure 7D) types.

Amphiboles in the studied metalherzolites are calcic in composition and have low contents of Al_2O_3 (<2.12 wt%) and Na_2O (<0.48 wt%), and high values of Mg# (0.92-1) (Table 4). Si values of this type of the analyzed

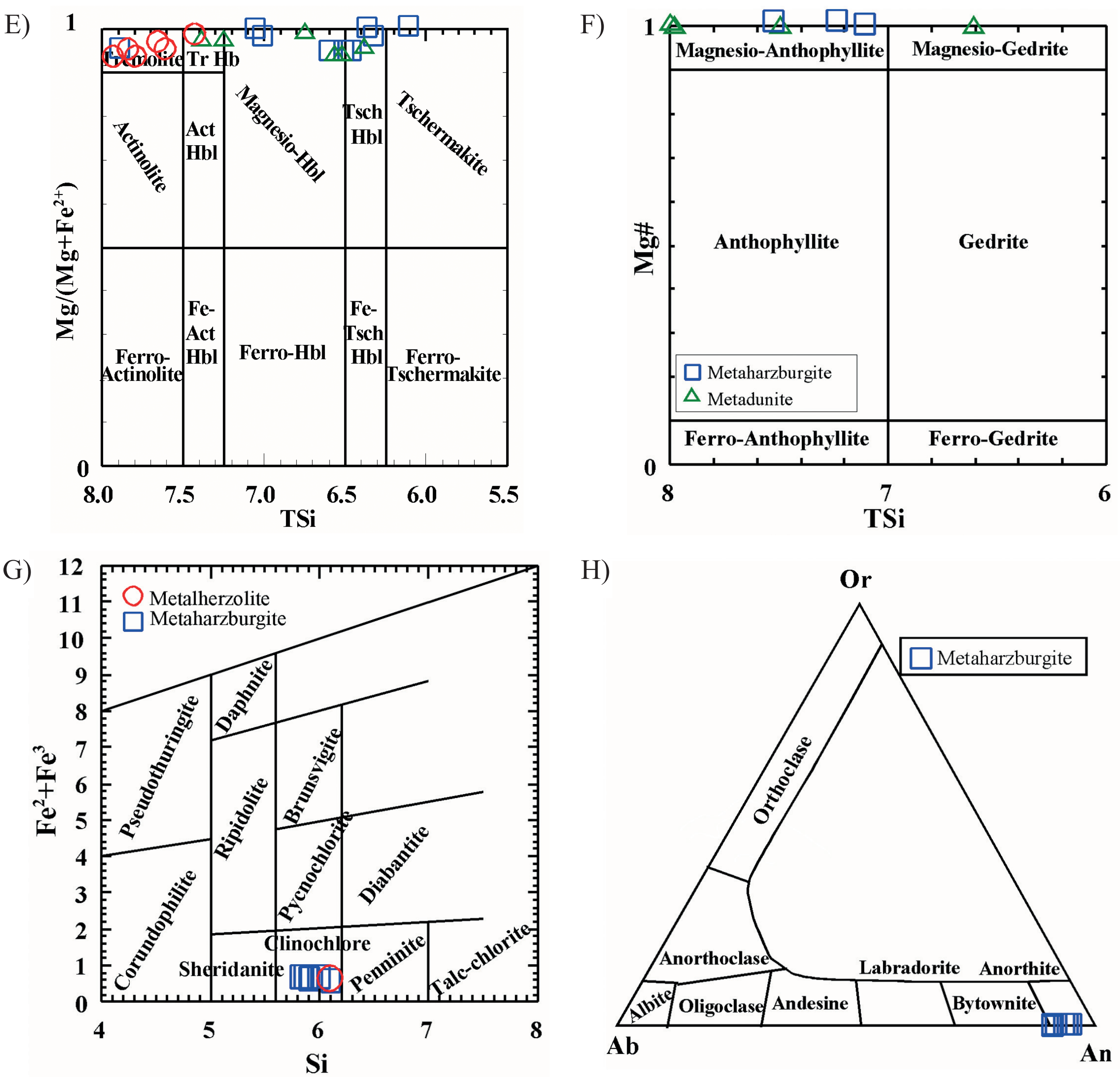

Figure 7. Continued. (E) Classification diagram of the Ca-amphiboles (Leake et al., 1997); (F) Classification diagram of the Fe-Mn-Mg orthorhombic amphiboles (Leake et al., 1997). (G) Chemical classification diagram of chlorites (Hey, 1954). The chlorites from the Kal-e-Kafi metaperidotites are clinochlore in composition.

amphiboles ranges from 6.94 to 8.02 apfu (atoms per formula unit). Chemical compositions of amphiboles in the metalherzolites, metaharzburgites and metadunites indicate that they are tremolite, tremolitic-hornblende, magnesio-hornblende, tschermakitic hornblende, tschermakite, magnesio-anthophyllite and magnesio-gedrite in composition (Figures 7E and F) (Leake et al., 1997).

Magnesian amphiboles can be found in the metaharzburgites and metadunites. They are magnesio-anthophyllite in composition (Figure 7F). MgO and Al_2O_3 values of the analyzed anthophyllites range from 30.64 to 41.83 and 0.1 to 3.68 (wt%), respectively. They have very low amount of Na_2O (0.01 to 0.68; average: 0.19 wt%) (Table 5).

Serpentine

The average Mg# content of the analyzed serpentines reaches up to 0.83 in metalherzolite, 0.90 in metaharzburgite and 0.91 in metadunites (Table 6). The average value of Cr_2O_3 in serpentines of the

Table 1. Electron microprobe analyses of olivines (wt%) in metaperidotites of the Kal-e-Kafi area and their calculated structural formula.

Sample	B804	B804	B807	B807	B707	B707	B707	B861	B861	B7071	B7071	B809	B809	B809	B809	B707
Analysis	190	191	273	275	174	187	188	175	176	215	219	203	204	207	209	172
Lithology	Metalherzolite				Metaharzburgite											
SiO_2	40.15	40.54	40.48	40.49	40.97	41.04	40.93	39.97	39.75	41.16	41.20	40.79	40.79	41.05	40.68	40.83
TiO_2	0.00	0.00	0.01	0.00	0.00	0.00	0.01	0.00	0.00	0.00	0.01	0.00	0.01	0.01	0.00	0.00
Al_2O_3	0.00	0.00	0.01	0.00	0.04	0.00	0.02	0.05	0.05	0.00	0.03	0.00	0.00	0.00	0.01	0.01
FeO*	9.75	8.78	13.33	13.10	10.53	10.34	10.44	10.09	10.15	9.07	8.98	11.88	11.81	11.61	12.44	10.78
MnO	0.22	0.16	0.36	0.34	0.09	0.14	0.11	0.08	0.06	0.08	0.09	0.30	0.29	0.29	0.29	0.12
MgO	49.90	50.70	45.31	45.62	48.25	48.28	47.88	49.83	49.67	49.50	49.16	46.87	46.95	46.81	46.19	47.95
CaO	0.00	0.00	0.01	0.00	0.00	0.02	0.00	0.00	0.00	0.01	0.01	0.08	0.02	0.01	0.03	0.01
Na_2O	0.00	0.00	0.01	0.00	0.00	0.00	0.00	0.01	0.01	0.00	0.00	0.01	0.00	0.00	0.01	0.00
K_2O	0.00	0.00	0.03	0.01	0.00	0.00	0.01	0.00	0.01	0.02	0.02	0.01	0.01	0.01	0.02	0.02
NiO	0.21	0.21	0.36	0.34	0.37	0.30	0.29	0.27	0.25	0.20	0.29	0.30	0.33	0.28	0.35	0.34
Total	100.23	100.39	99.91	99.90	100.26	100.12	99.69	100.31	99.94	100.04	99.78	100.23	100.21	100.07	100.02	100.05
								Oxygen#= 4								
Si	0.984	0.987	1.010	1.009	1.005	1.007	1.008	0.981	0.979	1.004	1.007	1.007	1.007	1.013	1.009	1.005
Al	0.000	0.000	0.000	0.000	0.001	0.000	0.001	0.002	0.001	0.000	0.001	0.000	0.000	0.000	0.000	0.000
Ti	0.000	0.000	0.000	0.000	0.000	0.000	0.000	0.000	0.000	0.000	0.000	0.000	0.000	0.000	0.000	0.000
Fe^{2+}	0.200	0.179	0.278	0.273	0.216	0.212	0.215	0.207	0.209	0.185	0.184	0.245	0.244	0.240	0.258	0.222
Mn	0.004	0.003	0.008	0.007	0.002	0.003	0.002	0.002	0.001	0.002	0.002	0.006	0.006	0.006	0.006	0.002
Mg	1.823	1.840	1.685	1.695	1.764	1.765	1.759	1.822	1.824	1.800	1.792	1.726	1.728	1.722	1.708	1.759
Ca	0.000	0.000	0.000	0.000	0.000	0.000	0.000	0.000	0.000	0.000	0.000	0.002	0.001	0.000	0.001	0.000
Na	0.000	0.000	0.001	0.000	0.000	0.000	0.000	0.000	0.000	0.000	0.000	0.000	0.000	0.000	0.000	0.000
K	0.000	0.000	0.001	0.000	0.000	0.000	0.000	0.000	0.000	0.000	0.001	0.000	0.000	0.000	0.001	0.001
Ni	0.004	0.004	0.007	0.007	0.007	0.006	0.006	0.005	0.005	0.004	0.006	0.006	0.007	0.006	0.007	0.007
Sum	3.015	3.013	2.990	2.991	2.995	2.993	2.991	3.019	3.019	2.995	2.993	2.992	2.993	2.987	2.990	2.996
Fe#	0.10	0.09	0.14	0.14	0.11	0.11	0.11	0.10	0.10	0.09	0.09	0.12	0.12	0.12	0.13	0.11
Mg#	0.90	0.91	0.86	0.86	0.89	0.89	0.89	0.90	0.90	0.91	0.91	0.88	0.88	0.88	0.87	0.89

Table 1. ...Continued

Sample	22-2a	22-2b	22-2b	22-2b	22-3a	22-3a	26-1a	26-1a	26-1a	26-1a	26-1a	26-2c	26-2c	26-1c	26-1b	26-3b
Analysis	11	11	12	13	1	2	10	11	6	6	7	6	5	8	11	16
Lithology	Metaharzburgite						Metadunite									
SiO_2	41.35	41.67	41.05	41.43	41.50	41.26	41.50	41.45	41.29	41.29	41.64	41.75	41.66	42.00	41.31	41.25
TiO_2	0.00	0.03	0.02	0.02	0.03	0.00	0.00	0.00	0.02	0.02	0.00	0.00	0.06	0.01	0.00	0.00
Al_2O_3	0.01	0.00	0.00	0.01	0.01	0.00	0.01	0.02	0.00	0.00	0.01	0.03	0.00	0.00	0.01	0.00
FeO*	8.56	8.77	9.04	9.38	9.50	8.41	8.91	8.86	8.84	8.84	9.00	8.93	10.04	9.19	8.82	9.50
MnO	0.22	0.25	0.24	0.19	0.14	0.17	0.15	0.14	0.22	0.22	0.11	0.17	0.15	0.14	0.13	0.24
MgO	50.11	50.39	50.30	50.45	50.00	49.49	49.75	49.16	49.14	49.14	49.17	49.52	50.47	50.03	48.96	49.69
CaO	0.03	0.00	0.00	0.07	0.04	0.03	0.03	0.00	0.06	0.06	0.00	0.05	0.02	0.00	0.02	0.01
Na_2O	0.00	0.00	0.00	0.05	0.00	0.00	0.01	0.00	0.00	0.00	0.00	0.02	0.00	0.00	0.01	0.00
K_2O	0.02	0.02	0.01	0.02	0.01	0.01	0.02	0.02	0.02	0.02	0.04	0.07	0.03	0.01	0.04	0.02
NiO	0.02	0.05	0.06	0.11	0.00	0.00	0.00	0.03	0.03	0.03	0.00	0.03	0.00	0.01	0.10	0.11
Total	100.25	101.23	100.71	101.63	101.15	99.37	100.45	99.68	99.62	99.62	99.97	100.52	102.41	100.41	99.40	100.82
Oxygen#= 4																
Si	1.00	1.00	1.00	1.00	1.00	1.01	1.01	1.01	1.01	1.01	1.01	1.01	1.00	1.01	1.01	1.00
Al	0.00	0.00	0.00	0.00	0.00	0.00	0.00	0.00	0.00	0.00	0.00	0.00	0.00	0.00	0.00	0.00
Ti	0.00	0.00	0.00	0.00	0.00	0.00	0.00	0.00	0.00	0.00	0.00	0.00	0.00	0.00	0.00	0.00
Fe^{2+}	0.17	0.18	0.18	0.19	0.19	0.17	0.18	0.18	0.18	0.18	0.18	0.18	0.20	0.19	0.18	0.19
Mn	0.01	0.01	0.01	0.00	0.00	0.00	0.00	0.00	0.01	0.01	0.00	0.00	0.00	0.00	0.00	0.01
Mg	1.81	1.81	1.82	1.81	1.80	1.81	1.80	1.79	1.79	1.79	1.79	1.79	1.80	1.79	1.79	1.80
Ca	0.00	0.00	0.00	0.00	0.00	0.00	0.00	0.00	0.00	0.00	0.00	0.00	0.00	0.00	0.00	0.00
Na	0.00	0.00	0.00	0.00	0.00	0.00	0.00	0.00	0.00	0.00	0.00	0.00	0.00	0.00	0.00	0.00
K	0.00	0.00	0.00	0.00	0.00	0.00	0.00	0.00	0.00	0.00	0.00	0.00	0.00	0.00	0.00	0.00
Ni	0.00	0.00	0.00	0.00	0.00	0.00	0.00	0.00	0.00	0.00	0.00	0.00	0.00	0.00	0.00	0.00
Sum	3.00	3.00	3.00	3.00	3.00	2.99	2.99	2.99	2.99	2.99	2.99	2.99	3.00	2.99	2.99	3.00
Fe#	0.09	0.09	0.09	0.09	0.10	0.09	0.09	0.09	0.09	0.09	0.09	0.09	0.10	0.09	0.09	0.10
Mg#	0.91	0.91	0.91	0.91	0.90	0.91	0.91	0.91	0.91	0.91	0.91	0.91	0.90	0.91	0.91	0.90

Table 2. Electron microprobe analyses of orthopyroxenes (wt%) in metaperidotites of the Kal-e-Kafi area and their calculated structural formula.

Sample	B807	B807	B707	B707	B707	B707	B707	B707	B7071	B861	B861	B861	B861	22-2b	22-2b	22-2b	B707
Analysis	270	276	170	173	175	176	185	190	218	166	167	171	172	27	28	29	168
Lithology	Metalherzolite								Metaharzburgite								
SiO_2	57.34	56.78	56.07	56.40	55.97	56.59	55.87	56.54	57.42	56.34	55.79	59.04	57.57	57.98	58.46	58.38	56.35
TiO_2	0.00	0.00	0.00	0.02	0.00	0.02	0.00	0.00	0.02	0.00	0.00	0.02	0.00	0.00	0.01	0.04	0.01
Al_2O_3	0.64	1.52	3.22	2.88	2.56	2.12	2.94	2.19	1.40	1.26	1.96	0.91	1.74	0.69	0.72	0.90	3.47
Cr_2O_3	0.18	0.22	0.34	0.08	0.48	0.22	0.21	0.20	0.02	0.00	0.16	0.15	0.17	0.18	0.15	0.17	0.40
FeO*	8.22	8.42	6.62	6.93	8.33	7.95	9.04	8.51	6.83	7.91	8.35	6.50	7.45	5.81	5.45	5.34	6.57
MnO	0.34	0.34	0.05	0.09	0.16	0.14	0.14	0.14	0.08	0.10	0.07	0.15	0.17	0.23	0.20	0.19	0.08
MgO	32.90	32.34	33.77	33.36	32.36	32.84	31.90	32.63	34.41	34.39	33.82	31.94	32.05	34.76	34.54	35.02	33.35
CaO	0.25	0.24	0.03	0.03	0.06	0.02	0.06	0.06	0.03	0.06	0.06	0.11	0.10	0.41	0.49	0.47	0.04
Na_2O	0.00	0.00	0.01	0.00	0.00	0.00	0.00	0.00	0.00	0.01	0.01	0.12	0.28	0.01	0.04	0.01	0.00
K_2O	0.02	0.02	0.00	0.01	0.01	0.01	0.02	0.02	0.03	0.00	0.00	0.00	0.02	0.02	0.00	0.03	0.02
NiO	0.11	0.11	0.06	0.07	0.05	0.03	0.04	0.05	0.10	0.04	0.07	0.11	0.09	0.05	0.00	0.00	0.07
Total	99.99	99.97	100.19	99.87	99.98	99.93	100.22	100.35	100.31	100.10	100.29	99.05	99.65	100.1	100.1	100.6	100.37
								Oxygen#= 6									
Si	1.998	1.981	1.931	1.952	1.950	1.967	1.946	1.962	1.975	1.944	1.927	2.074	2.008	1.994	2.011	1.996	1.940
Ti	0.000	0.000	0.000	0.001	0.000	0.000	0.000	0.000	0.000	0.000	0.000	0.000	0.000	0.000	0.000	0.001	0.000
Al^{VI}	0.002	0.019	0.069	0.048	0.050	0.033	0.054	0.038	0.025	0.051	0.073	0.000	0.000	0.006	0.000	0.004	0.060
Al^{IV}	0.024	0.043	0.061	0.069	0.055	0.054	0.066	0.051	0.032	0.000	0.006	0.038	0.072	0.022	0.029	0.032	0.081
Cr	0.005	0.006	0.009	0.002	0.013	0.006	0.006	0.006	0.000	0.000	0.004	0.004	0.005	0.005	0.004	0.005	0.011
Fe^{2+}	0.239	0.246	0.191	0.201	0.243	0.231	0.263	0.247	0.196	0.167	0.178	0.191	0.217	0.167	0.157	0.153	0.189
Fe^{3+}	0.000	0.000	0.000	0.000	0.000	0.000	0.000	0.000	0.000	0.061	0.063	0.000	0.000	0.000	0.000	0.000	0.000
Mn	0.010	0.010	0.002	0.003	0.005	0.004	0.004	0.004	0.002	0.003	0.002	0.004	0.005	0.007	0.006	0.006	0.002
Mg	1.709	1.682	1.734	1.721	1.681	1.702	1.656	1.648	1.764	1.770	1.741	1.673	1.667	0.972	0.966	0.962	1.712
Ca	0.009	0.009	0.001	0.001	0.002	0.001	0.002	0.002	0.001	0.002	0.002	0.004	0.004	0.015	0.018	0.017	0.002
Na	0.000	0.000	0.000	0.000	0.000	0.000	0.000	0.000	0.000	0.001	0.001	0.008	0.019	0.001	0.003	0.001	0.000
K	0.001	0.001	0.000	0.000	0.000	0.000	0.001	0.001	0.001	0.000	0.000	0.000	0.001	0.001	0.000	0.001	0.001
Ni	0.003	0.003	0.002	0.002	0.001	0.001	0.001	0.001	0.003	0.001	0.002	0.003	0.003	0.001	0.000	0.000	0.002
Sum	3.999	3.999	4.000	4.000	4.000	4.000	3.999	3.999	3.999	4.000	4.000	4.000	3.999	3.999	4.000	3.999	3.999
Q	1.957	1.937	1.926	1.923	1.926	1.934	1.922	1.937	1.962	1.939	1.921	1.868	1.888	1.964	1.947	1.955	1.903
J	0.000	0.000	0.001	0.000	0.000	0.000	0.000	0.000	0.000	0.001	0.002	0.017	0.038	0.001	0.005	0.001	0.000
WO	0.092	0.000	0.000	0.000	0.000	0.000	0.000	0.000	0.000	0.000	0.000	0.000	0.000	0.766	0.925	0.878	0.000
EN	87.268	86.103	86.898	87.267	84.571	86.303	83.627	85.255	88.773	88.778	87.370	89.156	87.331	90.42	90.74	91.05	86.771
FS	12.226	12.580	9.560	10.169	12.214	11.725	13.297	12.474	9.884	8.402	8.924	10.170	11.384	8.818	8.331	8.069	9.592
Fe#	0.12	0.13	0.10	0.11	0.13	0.12	0.14	0.13	0.10	0.09	0.09	0.10	0.12	0.15	0.14	0.14	0.10
Mg#	0.88	0.87	0.90	0.90	0.87	0.88	0.86	0.87	0.90	0.91	0.91	0.90	0.89	0.85	0.86	0.86	0.90

Table 2. ...Continued

Sample	22-3a	22-3a	22-3a	22-3a	22-3b	22-3b	22-3b	26-2a	26-2a	26-2a	26-2b	26-2b	26-2b	26-2b	26-2b	26-3a	26-3a
Analysis	5	6	8	9	6	7	8	13	14	19	11	12	13	7	8	10	12
Lithology	Metaharzburgite							Metadunite									
SiO_2	57.36	57.61	57.86	57.90	57.74	57.77	57.69	57.75	58.07	58.00	57.65	57.60	57.93	57.84	56.57	57.95	58.12
TiO_2	0.04	0.06	0.05	0.03	0.00	0.04	0.07	0.04	0.08	0.07	0.03	0.08	0.06	0.01	0.08	0.03	0.01
Al_2O_3	1.30	1.38	1.20	1.40	1.31	1.22	1.74	1.33	1.36	0.72	0.98	1.10	0.96	1.01	1.44	0.71	0.71
Cr_2O_3	0.05	0.22	0.11	0.12	0.18	0.10	0.33	0.36	0.33	0.23	0.11	0.30	0.22	0.17	0.22	0.16	0.13
FeO*	5.92	6.10	6.19	5.72	5.80	6.17	6.54	6.35	6.74	6.47	6.28	6.43	6.03	6.43	6.44	6.77	5.67
MnO	0.15	0.00	0.24	0.20	0.22	0.24	0.25	0.18	0.18	0.25	0.15	0.19	0.25	0.20	0.16	0.24	0.20
MgO	34.96	33.94	35.02	34.57	34.40	34.62	34.02	34.51	34.39	34.51	34.35	34.65	34.88	34.34	34.34	34.55	34.16
CaO	0.50	0.43	0.48	0.42	0.49	0.48	0.55	0.60	0.49	0.46	0.53	0.51	0.54	0.59	0.55	0.44	0.38
Na_2O	0.01	0.02	0.00	0.01	0.01	0.00	0.00	0.00	0.04	0.01	0.01	0.00	0.01	0.00	0.14	0.01	0.03
K_2O	0.01	0.01	0.00	0.03	0.03	0.04	0.02	0.01	0.03	0.01	0.00	0.02	0.04	0.01	0.07	0.03	0.03
NiO	0.00	0.00	0.01	0.10	0.06	0.01	0.00	0.00	0.02	0.00	0.00	0.00	0.03	0.00	0.01	0.01	0.04
Total	100.3	99.77	101.2	100.5	100.2	100.7	101.2	101.1	101.7	100.7	100.1	100.9	100.9	101.1	100.1	100.9	99.93
								Oxygen#= 6									
Si	1.966	1.992	1.970	1.984	1.985	1.977	1.971	1.971	1.973	1.988	1.986	1.970	1.977	1.973	1.948	1.984	2.002
Ti	0.001	0.002	0.001	0.001	0.000	0.001	0.002	0.001	0.002	0.002	0.001	0.002	0.002	0.000	0.002	0.001	0.000
Al^{VI}	0.034	0.008	0.030	0.016	0.015	0.023	0.029	0.029	0.027	0.012	0.014	0.030	0.023	0.027	0.052	0.016	0.000
Al^{IV}	0.018	0.049	0.018	0.040	0.038	0.027	0.041	0.025	0.028	0.017	0.026	0.014	0.016	0.014	0.006	0.012	0.029
Cr	0.001	0.006	0.003	0.003	0.005	0.003	0.009	0.010	0.009	0.006	0.003	0.008	0.006	0.005	0.006	0.004	0.004
Fe^{2+}	0.170	0.176	0.176	0.164	0.167	0.177	0.187	0.181	0.192	0.185	0.181	0.184	0.172	0.183	0.185	0.194	0.163
Fe^{3+}	0.000	0.000	0.000	0.000	0.000	0.000	0.000	0.000	0.000	0.000	0.000	0.000	0.000	0.000	0.000	0.000	0.000
Mn	0.004	0.000	0.007	0.006	0.006	0.007	0.007	0.005	0.005	0.007	0.004	0.006	0.007	0.006	0.005	0.007	0.006
Mg	0.979	0.944	0.978	0.953	0.956	0.969	0.948	0.965	0.961	0.974	0.970	0.976	0.976	0.981	0.985	0.982	0.966
Ca	0.018	0.016	0.018	0.015	0.018	0.018	0.020	0.022	0.018	0.017	0.020	0.019	0.020	0.022	0.020	0.016	0.014
Na	0.001	0.001	0.000	0.001	0.001	0.000	0.000	0.000	0.003	0.001	0.001	0.000	0.001	0.000	0.009	0.001	0.002
K	0.000	0.000	0.000	0.001	0.001	0.002	0.001	0.000	0.001	0.000	0.000	0.001	0.002	0.000	0.003	0.001	0.001
Ni	0.000	0.000	0.000	0.003	0.002	0.000	0.000	0.000	0.001	0.000	0.000	0.000	0.001	0.000	0.000	0.000	0.001
Sum	4.000	4.000	4.000	3.999	3.999	3.998	3.999	4.000	3.999	4.000	4.000	3.999	3.998	4.000	3.997	3.999	3.999
Q	1.974	1.942	1.971	1.945	1.947	1.961	1.940	1.959	1.952	1.966	1.965	1.969	1.966	1.975	1.968	1.973	1.955
J	0.001	0.003	0.000	0.001	0.001	0.000	0.000	0.000	0.005	0.001	0.001	0.000	0.001	0.000	0.019	0.001	0.004
WO	0.928	0.820	0.885	0.790	0.924	0.895	1.034	1.117	0.912	0.856	0.994	0.946	1.000	1.089	1.028	0.815	0.715
EN	90.28	90.10	89.86	90.51	90.22	89.78	90.10	89.39	89.04	89.38	89.60	89.46	89.91	89.360	89.337	89.045	90.655
FS	8.796	9.084	9.260	8.699	8.861	9.329	9.969	9.492	10.05	9.768	9.411	9.592	9.086	9.551	9.635	10.140	8.629
Fe#	0.15	0.16	0.15	0.15	0.15	0.15	0.16	0.16	0.17	0.16	0.16	0.16	0.15	0.16	0.16	0.17	0.14
Mg#	0.85	0.84	0.85	0.85	0.85	0.84	0.83	0.84	0.84	0.84	0.84	0.84	0.85	0.84	0.84	0.84	0.86

Table 3. Electron microprobe analyses of clinopyroxenes (wt%) in metaperidotites of the Kal-e-Kafi area and their calculated structural formula.

Sample	B708	B708	B708	B708	B807	B807	B807	B807	B807	B807	B807	B809	B809	B809	B809	B809	B809
Analysis	198	199	200	202	191	192	195	196	197	198	199	201	202	205	206	208	210
Lithology	Metalherzolite											Metaharzburgite					
SiO_2	54.84	54.98	55.32	55.23	56.07	56.20	56.07	56.11	56.13	56.01	56.32	55.17	54.77	55.62	54.98	55.85	55.72
TiO_2	0.00	0.00	0.00	0.00	0.00	0.00	0.00	0.00	0.00	0.03	0.00	0.09	0.12	0.06	0.00	0.00	0.00
Al_2O_3	0.07	0.07	0.19	0.20	0.05	0.03	0.10	0.05	0.10	0.11	0.10	1.44	2.08	0.59	1.10	0.65	0.57
Cr_2O_3	0.00	0.03	0.00	0.01	0.00	0.00	0.00	0.06	0.01	0.03	0.04	0.02	0.01	0.06	0.06	0.00	0.00
FeO*	1.22	1.21	1.20	1.04	1.45	0.94	0.95	0.91	1.12	1.10	0.99	1.91	1.92	1.40	1.88	1.73	1.67
MnO	0.12	0.07	0.10	0.10	0.09	0.08	0.08	0.08	0.09	0.12	0.08	0.08	0.08	0.09	0.04	0.05	0.08
MgO	18.04	17.91	17.84	18.11	17.35	17.64	17.63	17.60	17.39	17.48	17.69	16.66	16.59	17.10	16.99	17.09	17.29
CaO	25.76	25.51	25.71	25.69	24.74	24.90	24.93	24.83	24.67	24.85	25.05	24.96	24.67	24.78	25.05	24.80	24.56
Na_2O	0.00	0.00	0.00	0.00	0.01	0.00	0.02	0.00	0.02	0.01	0.00	0.01	0.01	0.00	0.00	0.00	0.00
K_2O	0.00	0.00	0.00	0.00	0.02	0.01	0.03	0.02	0.01	0.11	0.02	0.01	0.00	0.02	0.01	0.02	0.02
NiO	0.04	0.00	0.02	0.02	0.03	0.04	0.00	0.02	0.00	0.02	0.01	0.03	0.04	0.02	0.04	0.02	0.02
Total	100.1	99.8	100.4	100.4	99.8	99.9	99.8	99.7	99.6	99.9	100.3	100.4	100.3	99.7	100.2	100.2	99.94
Oxygens#= 6																	
Si	1.984	1.995	1.997	1.991	2.041	2.041	2.037	2.042	2.047	2.036	2.037	2.002	1.988	2.027	1.996	2.028	2.026
Ti	0.000	0.000	0.000	0.000	0.000	0.000	0.000	0.000	0.000	0.001	0.000	0.003	0.003	0.002	0.000	0.000	0.000
Al^{VI}	0.003	0.003	0.003	0.008	0.000	0.000	0.000	0.000	0.000	0.000	0.000	0.000	0.012	0.000	0.004	0.000	0.000
Al^{IV}	0.000	0.000	0.005	0.000	0.002	0.001	0.004	0.002	0.004	0.005	0.004	0.062	0.077	0.025	0.044	0.028	0.024
Cr	0.000	0.001	0.000	0.000	0.000	0.000	0.000	0.002	0.000	0.001	0.001	0.001	0.000	0.002	0.002	0.000	0.000
Fe^{2+}	0.007	0.031	0.036	0.022	0.044	0.029	0.029	0.028	0.034	0.033	0.030	0.057	0.058	0.042	0.057	0.053	0.051
Fe^{3+}	0.029	0.005	0.000	0.010	0.000	0.000	0.000	0.000	0.000	0.000	0.000	0.000	0.000	0.000	0.000	0.000	0.000
Mn	0.004	0.002	0.003	0.003	0.003	0.002	0.002	0.002	0.003	0.004	0.002	0.003	0.003	0.003	0.001	0.002	0.003
Mg	0.973	0.969	0.960	0.973	0.942	0.955	0.955	0.955	0.946	0.947	0.954	0.901	0.898	0.929	0.920	0.925	0.937
Ca	0.999	0.992	0.994	0.992	0.965	0.969	0.970	0.968	0.964	0.967	0.971	0.970	0.959	0.968	0.975	0.965	0.957
Na	0.000	0.000	0.000	0.000	0.001	0.000	0.001	0.000	0.001	0.000	0.000	0.000	0.001	0.000	0.000	0.000	0.000
K	0.000	0.000	0.000	0.000	0.001	0.000	0.002	0.001	0.000	0.005	0.001	0.000	0.000	0.001	0.001	0.001	0.001
Ni	0.001	0.000	0.001	0.000	0.001	0.001	0.000	0.000	0.000	0.001	0.000	0.001	0.001	0.001	0.001	0.000	0.001
Sum	4.000	4.000	4.000	4.000	3.999	4.000	3.998	3.999	4.000	3.995	3.999	4.000	4.000	3.999	3.999	3.999	3.999
Q	1.979	1.992	1.991	1.987	1.951	1.953	1.954	1.951	1.944	1.948	1.954	1.929	1.915	1.939	1.951	1.942	1.945
J	0.000	0.001	0.000	0.000	0.001	0.000	0.003	0.000	0.003	0.001	0.000	0.001	0.002	0.000	0.000	0.000	0.000
WO	49.64	49.56	49.79	49.47	49.42	49.61	49.58	49.53	49.54	49.52	49.59	50.25	49.44	49.78	49.66	49.66	49.18
EN	49.17	48.62	48.23	48.97	48.23	48.90	48.80	48.92	48.61	48.48	48.78	46.68	46.85	47.88	47.11	47.60	48.17
FS	0.361	1.564	1.823	1.085	2.259	1.466	1.469	1.419	1.753	1.714	1.527	2.995	3.038	2.196	2.917	2.708	2.605
Mg#	0.99	0.97	0.96	0.98	0.96	0.97	0.97	0.97	0.97	0.97	0.97	0.94	0.94	0.96	0.94	0.95	0.95

Table 3. ...Continued

Sample	22-1b	22-1b	22-1b	22-1b	22-2b	22-2b	26-2a	26-2b	26-2b	26-2b	26-2b	26-2b	26-2b
Analysis	20	21	22	23	20	22	9	1	2	3	4	5	6
Lithology	Metaharzburgite						Metadunite						
SiO_2	53.69	55.41	55.00	54.65	54.62	55.16	54.17	55.13	54.92	54.45	54.52	54.64	55.08
TiO_2	0.07	0.03	0.06	0.01	0.11	0.10	0.07	0.06	0.09	0.06	0.09	0.03	0.07
Al_2O_3	2.33	1.30	1.44	1.50	1.21	1.31	1.40	1.19	1.24	1.51	1.20	1.43	1.28
Cr_2O_3	0.34	0.08	0.21	0.29	0.28	0.36	0.42	0.24	0.16	0.29	0.32	0.31	0.26
FeO*	2.22	2.13	2.01	2.33	2.31	2.23	2.55	2.28	2.29	2.27	2.55	2.24	2.26
MnO	0.13	0.09	0.14	0.19	0.06	0.13	0.05	0.16	0.02	0.10	0.08	0.06	0.07
MgO	18.27	17.78	17.61	17.78	17.52	17.96	17.91	17.69	17.87	17.51	17.85	16.98	17.70
CaO	22.62	23.24	23.90	22.96	23.92	23.64	23.56	23.11	23.68	23.63	23.39	23.28	23.19
Na_2O	0.19	0.17	0.18	0.27	0.14	0.20	0.32	0.17	0.13	0.21	0.21	0.23	0.17
K_2O	0.04	0.02	0.02	0.03	0.02	0.01	0.02	0.04	0.01	0.01	0.04	0.03	0.02
NiO	0.03	0.00	0.00	0.03	0.04	0.07	0.00	0.00	0.04	0.02	0.00	0.00	0.00
Total	99.9	100.3	100.6	100.0	100.2	101.2	100.5	100.1	100.5	100.1	100.3	99.23	100.1
Oxygens#= 6													
Si	1.941	2.003	1.983	1.979	1.979	1.977	1.953	1.999	1.982	1.974	1.972	2.000	1.996
Ti	0.002	0.001	0.002	0.000	0.003	0.003	0.002	0.002	0.002	0.002	0.002	0.001	0.002
Al^{VI}	0.059	0.000	0.017	0.021	0.021	0.023	0.047	0.001	0.018	0.026	0.028	0.000	0.004
Al^{IV}	0.040	0.055	0.044	0.043	0.030	0.032	0.012	0.050	0.035	0.038	0.023	0.062	0.051
Cr	0.010	0.002	0.006	0.008	0.008	0.010	0.012	0.007	0.005	0.008	0.009	0.009	0.007
Fe^{2+}	0.067	0.064	0.059	0.071	0.059	0.067	0.065	0.069	0.069	0.064	0.074	0.067	0.068
Fe^{3+}	0.000	0.000	0.000	0.000	0.000	0.000	0.000	0.000	0.000	0.000	0.000	0.000	0.000
Mn	0.004	0.003	0.004	0.006	0.002	0.004	0.002	0.005	0.001	0.003	0.002	0.002	0.002
Mg	0.947	0.942	0.947	0.947	0.946	0.953	0.962	0.942	0.957	0.946	0.963	0.927	0.940
Ca	0.876	0.900	0.923	0.891	0.929	0.908	0.910	0.898	0.916	0.918	0.906	0.913	0.900
Na	0.013	0.012	0.013	0.019	0.010	0.014	0.022	0.012	0.009	0.015	0.015	0.016	0.012
K	0.002	0.001	0.001	0.001	0.001	0.000	0.001	0.002	0.000	0.000	0.002	0.001	0.001
Ni	0.001	0.000	0.000	0.001	0.001	0.002	0.000	0.000	0.001	0.001	0.000	0.000	0.000
Sum	3.998	3.999	3.999	3.999	3.999	4.000	3.999	3.998	4.000	4.000	3.998	3.999	3.999
Q	1.928	1.923	1.930	1.921	1.945	1.934	1.949	1.923	1.947	1.933	1.946	1.909	1.925
J	0.027	0.024	0.025	0.038	0.020	0.028	0.045	0.024	0.018	0.030	0.029	0.033	0.024
WO	45.35	46.75	47.72	46.23	47.70	46.84	46.64	46.57	47.03	47.41	46.52	47.80	46.72
EN	50.97	49.76	48.92	49.81	48.61	49.51	49.34	49.60	49.39	48.88	49.40	48.51	49.62
FS	3.68	3.49	3.35	3.96	3.69	3.65	4.02	3.84	3.58	3.71	4.08	3.69	3.67
Mg#	0.93	0.94	0.94	0.93	0.94	0.93	0.93	0.93	0.93	0.94	0.93	0.94	0.93

Table 4. Electron microprobe analyses of calcic-amphiboles (wt%) in metaperidotites of the Kal-e-Kafi area and their calculated structural formula.

Sample	B804	B804	B804	B804	B807	B807	B807	B807	B807	B807
Analysis	192	193	196	197	268	269	271	272	274	277
Lithology					Metalherzolie					
SiO_2	52.81	53.21	56.69	55.68	58.47	58.76	57.22	58.65	57.44	59.20
TiO_2	0.00	0.00	0.08	0.04	0.00	0.00	0.01	0.00	0.00	0.01
Al_2O_3	1.21	0.98	1.81	1.80	0.52	0.47	2.12	0.56	1.18	0.12
Cr_2O_3	0.20	0.21	0.40	0.31	0.14	0.03	0.32	0.22	0.17	0.00
FeO*	3.56	3.22	2.73	3.02	4.36	3.70	2.77	2.63	4.41	2.10
MnO	0.09	0.07	0.05	0.03	0.17	0.16	0.15	0.20	0.17	0.12
MgO	28.12	28.47	23.20	24.58	21.54	21.95	22.50	22.35	21.61	23.73
CaO	9.37	9.06	12.95	12.24	12.57	12.69	12.09	12.84	12.39	12.28
Na_2O	0.18	0.19	0.48	0.41	0.03	0.05	0.30	0.06	0.17	0.03
K_2O	0.05	0.03	0.06	0.04	0.03	0.03	0.07	0.04	0.05	0.04
Total	95.38	95.24	98.04	97.85	97.69	97.81	97.24	97.32	97.43	97.63
					Oxygen#= 23					
Si	6.909	6.936	7.668	7.442	7.994	8.017	7.751	8.012	7.860	7.968
Ti	0.000	0.000	0.008	0.004	0.000	0.000	0.001	0.000	0.000	0.001
Al^{VI}	0.000	0.000	0.000	0.000	0.077	0.075	0.090	0.089	0.050	0.000
Al^{IV}	0.186	0.150	0.289	0.283	0.006	0.000	0.249	0.000	0.140	0.020
Cr	0.020	0.022	0.042	0.033	0.015	0.003	0.034	0.024	0.018	0.000
Fe^{2+}	0.000	0.000	0.000	0.000	0.279	0.264	0.000	0.217	0.120	0.000
Fe^{3+}	0.390	0.351	0.309	0.337	0.219	0.158	0.314	0.083	0.385	0.236
Mn	0.010	0.007	0.006	0.004	0.020	0.018	0.017	0.023	0.020	0.014
Mg	5.486	5.533	4.677	4.897	4.390	4.465	4.544	4.552	4.408	4.761
Ca	1.313	1.266	1.876	1.753	1.841	1.855	1.755	1.880	1.817	1.770
Na	0.045	0.048	0.126	0.106	0.008	0.013	0.080	0.015	0.046	0.008
K	0.008	0.006	0.010	0.007	0.004	0.006	0.013	0.006	0.009	0.007
Sum	14.367	14.319	15.012	14.866	14.854	14.875	14.847	14.901	14.871	14.785
Mg#	1.00	1.00	1.00	1.00	0.94	0.94	1.00	0.98	0.92	1.00

metalherzolite and metaharzburgite (~0.14 wt%) is lower than the metadunites (~0.8 wt%) (Table 6). According to the X-ray diffraction analysis (XRD patterns), the main serpentine type in the studied metaperidotites identified as antigorite (Figure 6).

Talc

This mineral has high Mg# (0.8-0.98) and is a common mineral in the orthopyroxene- bearing rocks of the area (metaharzburgites). The Al_2O_3, FeO* and Na_2O contents of the analyzed talcs range 0.41 to 2.09, 0.1 to 7.36 and 0.04 to 0.52 wt%, respectively (Table 7). SiO_2 value in the analyzed talcs is nearly twice the MgO amount (Table 7).

Chlorite

Chlorites in the metaharzburgites have SiO_2 and Al_2O_3 values of 31.12-32.24 and 17.51-20.06 wt%, respectively, and FeO* and MgO amounts range from 2.76-3.25 and 31.26- 31.91 wt%, respectively. The Mg# of the analyzed chlorites is 0.945-0.954 (Table 8). The studied chlorites are plotted in the clinochlore field of classification diagram of chlorites (Hey, 1954) (Figure 7G).

Spinel

Spinels of the studied rocks show systematic compositional variation along their core to rim path. Spinel cores are enriched in Cr and depleted in Mg (Table 9). The Cr#, Mg# and TiO_2 value of chromian spinels

Table 4. ...Continued

Sample	22-1a	22-1a	22-1a	22-1a	22-1a	22-1a	22-1a	22-1b	22-1b	22-1b	22-1b	22-1b	22-1b	22-1c	22-1c	22-1c
Analysis	11	12	13	15	16	17	9	10	15	17	7	8	9	1	10	2
Lithology	Metaharzburgite															
SiO_2	44.70	45.24	46.16	45.97	47.09	46.70	45.55	46.10	45.79	45.97	45.92	47.09	45.83	47.53	46.52	46.11
TiO_2	0.35	0.67	0.47	0.64	0.43	0.59	0.65	0.53	0.60	0.53	0.52	0.40	0.63	0.58	0.40	0.46
Al_2O_3	12.14	11.42	11.25	11.33	11.07	11.45	11.44	11.48	11.57	11.72	11.03	10.51	11.47	10.09	10.25	11.41
Cr_2O_3	4.36	4.25	4.25	4.08	3.96	4.12	4.09	4.70	4.44	4.27	4.20	4.28	4.18	4.09	4.37	4.72
FeO*	1.07	1.89	2.01	1.09	1.05	1.15	1.91	1.73	1.67	1.55	1.81	1.70	1.75	1.77	1.70	2.02
MnO	0.09	0.12	0.14	0.08	0.10	0.15	0.07	0.07	0.05	0.11	0.01	0.09	0.08	0.05	0.10	0.06
MgO	19.01	18.29	18.93	18.62	19.18	18.29	18.20	18.67	18.83	19.01	18.50	19.30	18.55	19.33	18.85	18.50
CaO	11.45	11.60	12.09	12.33	12.29	12.53	12.10	12.09	11.95	11.75	11.51	11.97	12.19	12.19	11.92	12.07
Na_2O	1.70	2.69	2.45	1.51	1.54	1.53	2.64	2.75	2.71	2.26	2.60	2.15	2.31	2.36	2.32	2.62
K_2O	0.48	0.59	0.41	0.66	0.61	0.65	0.45	0.43	0.53	0.52	0.55	0.40	0.55	0.47	0.28	0.46
Total	94.39	95.14	96.26	95.33	96.57	96.11	95.57	96.93	96.57	96.44	94.97	96.30	96.07	96.80	95.10	96.85
	Oxygen#=23															
Si	6.305	6.420	6.436	6.503	6.564	6.572	6.462	6.430	6.400	6.398	6.501	6.545	6.447	6.607	6.568	6.441
Ti	0.037	0.072	0.049	0.068	0.045	0.062	0.069	0.056	0.063	0.055	0.055	0.042	0.067	0.061	0.042	0.048
Al^{IV}	1.695	1.580	1.564	1.497	1.436	1.428	1.538	1.570	1.600	1.602	1.499	1.455	1.553	1.393	1.432	1.559
Al^{VI}	0.321	0.329	0.283	0.391	0.381	0.470	0.374	0.315	0.304	0.320	0.340	0.265	0.347	0.258	0.272	0.318
Cr	0.119	0.212	0.221	0.122	0.116	0.128	0.214	0.191	0.184	0.170	0.202	0.187	0.194	0.194	0.190	0.223
Fe^{2+}	0.000	0.000	0.000	0.000	0.000	0.092	0.160	0.029	0.000	0.000	0.000	0.000	0.018	0.006	0.000	0.034
Fe^{3+}	0.514	0.504	0.496	0.483	0.462	0.393	0.325	0.519	0.519	0.497	0.497	0.497	0.474	0.469	0.516	0.517
Mn	0.011	0.014	0.017	0.010	0.012	0.018	0.008	0.008	0.006	0.013	0.001	0.011	0.010	0.006	0.012	0.007
Mg	3.997	3.869	3.935	3.927	3.985	3.837	3.849	3.882	3.923	3.945	3.904	3.999	3.890	4.005	3.968	3.852
Ca	1.730	1.764	1.806	1.869	1.835	1.889	1.839	1.807	1.790	1.752	1.746	1.782	1.837	1.815	1.803	1.806
Na	0.195	0.504	0.468	0.283	0.252	0.307	0.566	0.550	0.524	0.362	0.459	0.362	0.467	0.451	0.438	0.516
K	0.086	0.107	0.073	0.119	0.108	0.117	0.081	0.077	0.095	0.092	0.099	0.071	0.099	0.083	0.050	0.082
Sum	15.28	15.61	15.54	15.40	15.36	15.42	15.65	15.63	15.62	15.46	15.56	15.43	15.57	15.54	15.49	15.60

Table 5. Electron microprobe analyses of anthophyllite (wt%) in metaperidotites of the Kal-e-Kafi area and their calculated structural formula.

Sample	B707	B861	B861	B801	B801	B801	B801
Analysis	186	168	170	179	180	184	186
Lithology	Metaharzburgite			Metadunite			
SiO_2	55.02	49.79	52.20	58.55	53.79	42.53	58.50
TiO_2	0.00	0.17	0.01	0.00	0.00	0.00	0.00
Al_2O_3	1.64	3.68	0.74	0.29	0.19	0.10	0.53
FeO*	3.25	5.80	6.41	1.70	1.98	5.23	1.77
Cr_2O_3	0.33	0.35	0.10	0.04	0.00	0.06	0.01
MnO	0.01	0.04	0.14	0.00	0.05	0.10	0.00
MgO	31.83	30.64	31.73	32.19	34.31	41.86	31.78
CaO	0.00	0.01	0.06	0.00	0.02	0.01	0.02
Na_2O	0.05	0.86	0.07	0.12	0.06	0.01	0.17
K_2O	0.02	0.19	0.02	0.00	0.01	0.01	0.06
Total	91.82	91.18	91.38	92.85	90.41	89.85	92.83
Oxygens#= 23							
Si	7.685	7.106	7.387	8.107	7.549	5.822	8.124
Ti	0.000	0.018	0.001	0.000	0.000	0.000	0.000
Al	0.270	0.619	0.123	0.047	0.031	0.016	0.087
Cr	0.036	0.039	0.011	0.004	0.000	0.006	0.001
Fe^{3+}	0.306	0.417	0.268	0.197	0.232	0.599	0.206
Fe^{2+}	0.073	0.000	0.000	0.000	0.000	0.000	0.000
Mn	0.001	0.005	0.017	0.000	0.006	0.012	0.000
Mg	6.628	6.519	6.693	6.644	7.178	8.544	6.579
Ca	0.000	0.002	0.009	0.000	0.003	0.001	0.003
Na	0.014	0.238	0.019	0.032	0.016	0.003	0.046
K	0.004	0.035	0.004	0.000	0.002	0.002	0.011
Sum	15.017	15.273	15.023	15.032	15.018	15.004	15.056
Mg#	0.99	1.00	1.00	1.00	1.00	1.00	1.00

in the metaharzburgites and metadunites are 0.64-0.72, 0.24-0.31, 0.1-0.32 (wt%), and 0.65-0.7, 0.20-0.24, 0.1-0.2 (wt%), respectively (Table 9). All Cr-spinels in metalherzolites have been converted to magnetite (Table 9).

Plagioclase

All plagioclases in the metaharzburgites have anorthite composition (Average: $An_{93}Ab_{6.9}Or_{0.1}$) (Figure 7H; Table 12). Anorthite content of plagioclases in the gabbros varies from 83.8 to 94.2% (Average: 91.6%).

DISCUSSION

Contact metamorphism

The Kal-e-Kafi intrusive body comprises the four phases of magma intrusion ranging in composition from gabbro to diorite, monzonite and granite (Figure 2; Ahmadian et al., 2016; Salim et al., 2018). The Ti-in-biotite thermometer of the Kal-e-Kafi granitoids shows the crystallization temperature of 707 to 761 °C (average 745 °C; Salim, 2019).

The intrusion of the Eocene Kal-e-Kafi pluton increases the thermal gradient of the surrounding rocks leading to contact metamorphism in the surrounding rock units as skarn, hornfels and metaperidotites at the expense of the host rocks (Ranjbar et al., 2016).

Metamorphic evolution of metaperidotites

The presence of fine magnetite inclusions in the olivine neoblasts of metaharburgites indicate probably reveals that the magnetite inclusions have formed by partially serpentinization of primary olivines and pyroxens by

Table 6. Electron microprobe analyses of serpentines (wt%) in metaperidotites of the Kal-e-Kafi area and their calculated structural formula.

Sample	22-1a	22-1a	22-1a	22-1a	22-2a	22-2a	22-2a	22-2a	22-2b	22-2b	22-2b	22-2b	22-3a	B708	B807	B807
Analysis	24	25	26	27	12	13	14	15	31	32	33	34	23	201	193	200
Lithology	Metaharzburgite													Metalherzolite		
SiO_2	39.02	40.44	40.57	41.77	39.73	39.28	40.05	41.73	38.73	39.84	40.92	39.51	40.51	42.28	40.63	43.76
TiO_2	0.07	0.06	0.00	0.00	0.03	0.04	0.05	0.00	0.04	0.00	0.05	0.00	0.00	0.00	0.00	0.00
Al_2O_3	2.86	1.54	0.93	0.61	0.98	0.21	0.14	0.28	0.31	0.25	0.79	0.18	0.10	0.16	4.49	0.12
Cr_2O_3	0.98	0.00	0.03	0.00	0.04	0.00	0.00	0.04	0.00	0.02	0.01	0.00	0.00	0.17	0.11	0.00
FeO*	3.14	2.48	3.58	2.08	3.54	4.66	3.63	1.92	5.08	4.41	3.01	4.49	4.46	2.45	3.48	1.13
MnO	0.21	0.04	0.19	0.05	0.07	0.04	0.08	0.01	0.07	0.04	0.04	0.04	0.07	0.10	0.10	0.06
MgO	37.98	39.22	38.75	38.84	39.57	38.87	39.10	39.86	38.47	38.31	39.90	40.09	39.21	40.88	37.28	39.95
CaO	0.03	0.03	0.09	0.03	0.02	0.05	0.01	0.04	0.05	0.05	0.01	0.01	0.05	0.03	0.04	0.04
Na_2O	0.00	0.01	0.04	0.00	0.00	0.00	0.00	0.01	0.01	0.01	0.02	0.00	0.04	0.00	0.01	0.01
K_2O	0.03	0.03	0.03	0.00	0.03	0.04	0.02	0.01	0.05	0.02	0.02	0.03	0.02	0.00	0.46	0.02
Total	84.31	83.84	84.22	83.38	83.99	83.20	83.08	83.89	82.81	82.94	84.77	84.35	84.45	86.22	86.66	85.24
Oxygen#= 7																
Si	1.899	1.961	1.973	2.026	1.940	1.951	1.977	2.013	1.939	1.977	1.970	1.935	1.976	1.716	1.641	1.797
Ti	0.003	0.002	0.000	0.000	0.001	0.002	0.002	0.000	0.002	0.000	0.002	0.000	0.000	0.000	0.000	0.000
Al	0.164	0.088	0.054	0.035	0.056	0.012	0.008	0.016	0.018	0.015	0.045	0.011	0.006	0.009	0.242	0.006
Cr	0.038	0.000	0.001	0.000	0.001	0.000	0.000	0.001	0.000	0.001	0.000	0.000	0.000	0.009	0.006	0.000
Fe^{2+}	0.128	0.101	0.146	0.084	0.144	0.194	0.150	0.077	0.213	0.183	0.121	0.184	0.182	0.199	0.281	0.093
Mn	0.009	0.002	0.008	0.002	0.003	0.002	0.003	0.000	0.003	0.002	0.002	0.002	0.003	0.008	0.008	0.005
Mg	2.755	2.836	2.810	2.808	2.881	2.877	2.877	2.867	2.871	2.834	2.863	2.927	2.851	3.319	3.011	3.281
Ca	0.001	0.001	0.005	0.002	0.001	0.003	0.000	0.002	0.003	0.003	0.000	0.001	0.002	0.003	0.003	0.003
Na	0.000	0.001	0.003	0.000	0.000	0.000	0.000	0.001	0.001	0.001	0.002	0.000	0.003	0.000	0.002	0.001
K	0.002	0.002	0.002	0.000	0.002	0.003	0.002	0.000	0.003	0.001	0.001	0.002	0.001	0.000	0.074	0.003
Sum	4.998	4.994	5.002	4.957	5.030	5.043	5.018	4.979	5.052	5.016	5.007	5.061	5.024	5.275	5.273	5.202
Mg#	0.96	0.97	0.95	0.97	0.92	0.94	0.95	0.97	0.93	0.94	0.96	0.95	0.95	0.94	0.91	0.97

Table 6. Electron microprobe analyses of serpentines (wt%) in metaperidotites of the Kal-e-Kafi area and their calculated structural formula.

Sample	26-1a	26-1a	26-1a	26-1a	26-1a	26-1a	26-1b	26-1b	26-1b	26-1c	26-1c	26-2a	26-2a	26-2a	26-2b	26-2b	26-2c	26-2c
Analysis	15	16	17	18	19	20	13	14	15	11	12	20	21	22	14	15	11	12
Lithology	Metadunite																	
SiO_2	38.28	39.65	40.95	39.75	35.91	39.20	40.85	36.26	37.68	40.44	42.05	41.39	41.39	41.39	40.36	40.36	39.83	53.65
TiO_2	0.01	0.01	0.05	0.00	0.06	0.00	0.35	0.10	0.01	0.00	0.05	0.01	0.02	0.00	0.06	0.06	0.05	0.00
Al_2O_3	1.15	1.33	0.11	0.81	8.77	0.31	11.68	9.50	7.11	0.14	1.36	0.11	0.08	0.24	0.29	0.29	0.75	1.23
Cr_2O_3	0.01	0.00	0.02	0.08	0.36	0.00	1.70	0.61	0.52	0.00	0.10	0.06	0.00	0.06	0.00	0.00	0.29	0.23
FeO*	7.44	7.24	3.15	6.34	9.38	7.25	4.09	9.73	8.90	3.68	3.78	4.11	3.57	7.72	8.52	7.41	6.90	2.25
MnO	0.19	0.37	0.09	0.25	0.62	0.50	0.28	0.51	0.46	0.06	0.01	0.00	0.02	0.26	0.33	0.41	0.30	0.01
MgO	35.09	35.21	39.00	36.57	30.23	35.64	26.95	29.53	31.46	39.42	37.56	39.62	40.23	34.18	34.14	34.80	33.98	30.67
CaO	0.01	0.00	0.03	0.06	0.37	0.08	0.21	0.40	0.43	0.05	0.05	0.02	0.02	0.06	0.08	0.16	0.10	0.06
Na_2O	0.01	0.02	0.00	0.01	0.09	0.01	0.05	0.10	0.04	0.02	0.04	0.00	0.00	0.00	0.01	0.01	0.00	0.33
K_2O	0.03	0.06	0.03	0.03	0.38	0.00	5.83	0.29	0.08	0.01	0.03	0.01	0.03	0.03	0.00	0.03	0.04	0.04
Total	82.22	83.89	83.42	83.90	86.15	82.99	91.98	87.02	86.68	83.82	85.01	85.31	85.36	83.94	83.78	83.52	82.23	88.47
	Oxygen#= 7																	
Si	1.951	1.974	2.003	1.971	1.770	1.979	1.872	1.769	1.834	1.978	2.017	1.990	1.985	2.055	2.022	2.019	2.017	2.380
Ti	0.000	0.000	0.002	0.000	0.002	0.000	0.012	0.004	0.000	0.000	0.002	0.000	0.001	0.000	0.002	0.002	0.002	0.000
Al	0.069	0.078	0.006	0.047	0.509	0.019	0.631	0.546	0.408	0.008	0.077	0.006	0.005	0.014	0.017	0.017	0.045	0.065
Cr	0.000	0.000	0.001	0.003	0.014	0.000	0.062	0.023	0.020	0.000	0.004	0.002	0.000	0.002	0.000	0.000	0.012	0.008
Fe^{+2}	0.317	0.302	0.129	0.263	0.387	0.306	0.157	0.397	0.362	0.150	0.151	0.165	0.143	0.321	0.357	0.310	0.292	0.083
Mn	0.008	0.016	0.004	0.011	0.026	0.021	0.011	0.021	0.019	0.002	0.001	0.000	0.001	0.011	0.014	0.017	0.013	0.000
Mg	2.666	2.614	2.844	2.704	2.222	2.682	1.842	2.148	2.283	2.874	2.685	2.840	2.876	2.530	2.550	2.595	2.566	2.029
Ca	0.001	0.000	0.002	0.003	0.019	0.004	0.011	0.021	0.023	0.003	0.003	0.001	0.001	0.003	0.004	0.009	0.005	0.003
Na	0.000	0.002	0.000	0.001	0.008	0.001	0.004	0.010	0.004	0.002	0.004	0.000	0.000	0.000	0.001	0.001	0.000	0.029
K	0.002	0.004	0.002	0.002	0.024	0.000	0.341	0.018	0.005	0.001	0.002	0.000	0.002	0.002	0.000	0.002	0.003	0.002
Sum	5.015	4.989	4.992	5.005	4.982	5.013	4.942	4.956	4.957	5.019	4.944	5.005	5.013	4.938	4.968	4.972	4.954	4.599
Mg#	0.89	0.90	0.96	0.91	0.85	0.90	0.92	0.84	0.86	0.95	0.95	0.95	0.96	0.89	0.88	0.89	0.90	0.96

Table 7. Electron microprobe analyses of talcs (wt%) in metaperidotites of the Kal-e-Kafi area and their calculated structural formula.

Sample	B7071	B7071	B7071	B7071	B7071	B707	B707	B707	B707	B707	B707	B707	22-1a	22-2b	22-2a	22-2a	B801
Analysis	213	214	216	217	222	178	179	180	181	182	183	184	14	16	23	28	181
Lithology	Metaharzburgite													Metalherzolite			MDu
SiO_2	60.12	60.55	59.39	59.44	60.63	59.78	57.35	56.90	59.45	59.14	58.89	58.68	58.80	60.33	58.56	60.52	61.25
TiO_2	0.00	0.00	0.02	0.00	0.04	0.03	0.01	0.00	0.01	0.01	0.01	0.00	0.07	0.05	0.05	0.02	0.00
Al_2O_3	0.63	0.70	1.32	0.87	0.41	1.19	2.09	1.99	1.11	1.44	1.85	0.44	0.62	1.01	1.56	0.95	0.42
Cr_2O_3	0.07	0.07	0.19	0.00	0.08	0.05	0.24	0.07	0.11	0.17	0.10	0.05	0.12	0.11	0.24	0.16	0.00
FeO*	6.30	5.80	5.95	6.60	5.66	6.60	3.78	5.23	6.73	7.19	7.33	7.36	1.82	1.91	1.10	1.48	1.50
MnO	0.11	0.07	0.09	0.11	0.12	0.16	0.05	0.09	0.18	0.16	0.19	0.23	0.09	0.08	0.00	0.00	0.02
MgO	30.73	30.92	30.18	30.24	30.88	30.22	30.72	31.47	30.22	30.07	29.87	31.24	31.23	29.94	30.58	31.05	31.36
CaO	0.11	0.06	0.16	0.11	0.08	0.08	0.00	0.03	0.13	0.18	0.15	0.22	0.27	0.03	0.04	0.04	0.02
Na_2O	0.09	0.08	0.21	0.14	0.10	0.17	0.16	0.06	0.14	0.18	0.24	0.04	0.18	0.52	0.25	0.34	0.14
K_2O	0.02	0.02	0.02	0.02	0.01	0.00	0.04	0.29	0.02	0.02	0.02	0.01	0.04	0.01	0.05	0.04	0.03
Total	98.30	98.38	97.67	97.64	98.07	98.40	94.52	96.19	98.23	98.77	98.84	98.65	93.23	93.98	92.41	94.60	94.83
Oxygen#= 21																	
Si	6.422	6.462	6.385	6.392	6.491	6.378	6.370	6.211	6.355	6.287	6.256	6.246	7.368	7.475	7.362	7.439	6.782
Ti	0.000	0.000	0.002	0.000	0.005	0.003	0.001	0.000	0.001	0.001	0.001	0.000	0.007	0.005	0.005	0.002	0.000
Al	0.090	0.099	0.189	0.124	0.059	0.169	0.310	0.290	0.158	0.203	0.261	0.063	0.092	0.147	0.231	0.138	0.062
Cr	0.010	0.010	0.027	0.000	0.012	0.007	0.036	0.010	0.015	0.024	0.014	0.007	0.011	0.011	0.023	0.015	0.000
Fe^{2+}	1.347	1.238	1.280	1.420	1.213	1.409	0.841	1.143	1.438	1.528	1.558	1.567	0.191	0.198	0.116	0.152	0.333
Mn	0.023	0.015	0.020	0.024	0.025	0.034	0.010	0.019	0.037	0.035	0.041	0.048	0.009	0.008	0.000	0.000	0.004
Mg	6.565	6.599	6.490	6.504	6.613	6.448	6.825	6.871	6.460	6.393	6.346	6.651	5.834	5.530	5.731	5.688	6.945
Ca	0.024	0.013	0.034	0.023	0.018	0.017	0.001	0.006	0.028	0.039	0.031	0.047	0.036	0.004	0.005	0.006	0.004
Na	0.040	0.035	0.089	0.058	0.041	0.071	0.072	0.026	0.061	0.075	0.104	0.017	0.044	0.124	0.060	0.081	0.062
K	0.009	0.008	0.009	0.010	0.006	0.000	0.016	0.127	0.010	0.010	0.010	0.003	0.007	0.002	0.008	0.006	0.013
Sum	14.553	14.504	14.554	14.580	14.493	14.566	14.500	14.715	14.593	14.641	14.663	14.730	13.599	13.504	13.541	13.527	14.224
Mg#	0.83	0.84	0.84	0.82	0.85	0.82	0.89	0.86	0.82	0.81	0.80	0.81	0.97	0.97	0.98	0.97	0.95

Table 8. Electron microprobe analyses of chlorites and plagioclases (wt%) from metaharzburgites of the Kal-e-Kafi area and their calculated structural formula.

Sample	B7071	B707	B707	B707	B707	B707
Analysis	220	167	169	171	177	189
Mineral	Chlorite					
SiO_2	32.24	31.33	31.33	31.12	31.51	31.92
TiO_2	0.04	0.08	0.04	0.09	0.11	0.10
Al_2O_3	17.51	19.60	19.69	20.06	19.54	18.81
Cr_2O_3	1.71	0.59	0.80	0.73	0.67	0.64
FeO*	2.76	3.11	3.23	3.25	3.15	3.24
MnO	0.01	0.02	0.01	0.01	0.01	0.00
MgO	31.91	31.26	31.52	31.30	31.25	31.61
CaO	0.01	0.00	0.01	0.00	0.02	0.01
Na_2O	0.00	0.01	0.00	0.00	0.00	0.00
K_2O	0.01	0.00	0.02	0.01	0.02	0.00
Total	86.19	85.98	86.64	86.56	86.28	86.32
	Oxygen#=28					
Si	6.123	5.954	5.919	5.884	5.970	6.045
Ti	0.006	0.011	0.006	0.013	0.016	0.014
Al^{IV}	1.877	2.046	2.081	2.116	2.030	1.955
Al^{VI}	2.040	2.340	2.300	2.349	2.329	2.240
Cr	0.256	0.088	0.119	0.108	0.099	0.095
Fe^{2+}	0.438	0.493	0.510	0.513	0.498	0.514
Mn	0.002	0.003	0.002	0.001	0.002	0.000
Mg	9.034	8.855	8.877	8.823	8.827	8.924
Ca	0.001	0.001	0.002	0.000	0.004	0.001
Na	0.000	0.003	0.000	0.000	0.000	0.000
K	0.002	0.000	0.005	0.003	0.005	0.001
Sum	19.779	19.794	19.821	19.810	19.780	19.789
Fe^{2+}#	0.05	0.05	0.05	0.06	0.05	0.05
Mg#	0.95	0.95	0.95	0.95	0.95	0.95

Sample	22-3a	22-3a	22-3a	22-3b	22-3b	22-3b
Analysis	20	21	22	1	2	3
	Plagioclase					
SiO_2	45.28	46.11	45.42	44.52	44.89	44.54
TiO_2	0.03	0.02	0.06	0.04	0.02	0.00
Al_2O_3	35.66	35.41	35.02	35.33	35.53	34.94
FeO*	0.14	0.18	0.16	0.21	0.25	0.13
MnO	0.00	0.02	0.07	0.01	0.00	0.08
MgO	0.03	0.03	0.00	0.01	0.00	2.06
CaO	18.93	18.41	18.58	19.00	19.29	17.21
Na_2O	0.75	0.98	0.92	0.66	0.58	0.93
K_2O	0.01	0.02	0.02	0.02	0.02	0.00
Total	100.83	101.18	100.25	99.80	100.58	99.89
	Oxygen#=8					
Si	2.072	2.099	2.090	2.061	2.063	2.054
Ti	0.001	0.001	0.002	0.001	0.001	0.000
Al	1.922	1.898	1.898	1.926	1.923	1.898
Fe^{3+}	0.005	0.007	0.006	0.008	0.010	0.005
Mn	0.000	0.001	0.003	0.000	0.000	0.003
Mg	0.002	0.002	0.000	0.001	0.000	0.142
Ca	0.928	0.898	0.916	0.943	0.950	0.850
Na	0.067	0.086	0.082	0.059	0.052	0.083
K	0.001	0.001	0.001	0.001	0.001	0.000
Sum	4.998	4.993	4.998	5.000	5.000	5.035
Ab	6.70	8.70	8.20	5.90	5.20	8.90
An	93.20	91.20	91.70	94.00	94.70	91.10
Or	0.10	0.10	0.10	0.10	0.10	0.00

initial retrograde hydration of peridotites (M1) (Oliver et al., 1972; Paktunc, 1984). During the progressive metamorphism (M2), magnetites have been surrounded by metamorphic olivines (Nozaka, 2003, 2005; Khedr and Arai, 2012). Partial serpentinization of some olivine neoblasts and formation of late-stage chlorites around of the tremolites indicate occurrence of a retrograde metamorphism (M3) (Trommsdorff and Evans, 1980) after prograde metamorphism.

According to the following reactions, metamorphic olivines (neoblasts) may be formed during progressive metamorphism of metaperidotites (Spear, 1995):

$$\text{Brucite} + \text{Antigorite} \rightarrow 2\ \text{Forsterite} + 3\ H_2O \qquad (1)$$

$$2\ \text{Diopside} + 5\ \text{Antigorite} \rightarrow 6\ \text{Forsterite} + \text{Tremolite} + 9\ H_2O \qquad (2)$$

$$5\ \text{Antigorite} \rightarrow 6\ \text{Forsterite} + \text{Talc} + 9\ H_2O \qquad (3)$$

Chemical composition of olivines in peridotites is likely controlled by whole-rock chemistry and the grade of metamorphism (Mancini et al., 1996; Paktunc, 1984). According to DeHoog et al. (2010) the calcium content in olivine structure is dependent on temperature. During metamorphism, the low equilibrium temperature of the metamorphic olivines will cause to decreasing the CaO content (CaO<0.02 wt%) in comparison to the igneous olivines (CaO>0.04 wt%). Therefore, the very low CaO content of olivines in the studied metaperidotites indicates

Table 9. Electron microprobe analyses of spinels (wt%) in metaperidotites of the Kal-e-Kafi area and their calculated structural formula.

Sample	22-2a	22-2a	22-2a	22-2b	22-2b	22-3b	22-3b	22-2a	22-2b	22-2b	22-2b	22-2b	22-2b	22-2b	22-2b	22-2b
Analysis	17	18	19	2	7	13	15	20	1	3	4	5	6	8	9	10
Lithology	Metaharzburgite															
Comment	Core						Rim									
SiO_2	0.20	2.37	0.20	0.01	1.04	0.03	0.11	0.21	0.01	0.01	0.30	0.35	0.06	0.50	0.01	0.25
TiO_2	0.27	0.32	0.27	0.26	0.27	0.17	0.05	0.13	0.28	0.25	0.16	0.14	0.19	0.24	0.13	0.07
Al_2O_3	15.00	12.59	14.99	20.96	15.18	15.41	17.68	14.68	19.52	18.69	19.13	20.65	19.18	13.50	19.74	19.69
Cr_2O_3	49.18	47.69	44.97	42.37	45.07	48.94	46.08	47.83	42.24	44.49	42.07	41.15	44.37	43.24	43.51	40.56
FeO*	26.59	25.61	26.49	23.92	27.13	25.69	24.67	27.27	25.16	25.99	27.19	25.45	25.27	27.03	26.45	26.35
MnO	0.57	0.40	0.41	0.45	0.46	0.45	0.55	0.45	0.44	0.48	0.52	0.50	0.51	0.44	0.41	0.41
MgO	8.47	11.38	9.69	11.19	10.45	9.47	9.64	9.25	11.08	10.76	10.24	11.64	10.38	7.59	10.38	10.69
CaO	0.11	0.08	0.09	0.00	0.05	0.00	0.03	0.07	0.03	0.03	0.02	0.16	0.13	0.14	0.03	0.33
ZnO	0.24	0.07	0.22	0.20	0.30	0.11	0.42	0.00	0.08	0.12	0.25	0.07	0.00	0.11	0.22	0.20
Total	100.63	100.51	100.63	99.36	99.94	100.26	99.22	99.89	98.83	100.82	99.87	100.10	100.10	92.79	100.86	98.54
	Oxygen#=32															
Si	0.053	0.605	0.053	0.003	0.266	0.007	0.027	0.056	0.002	0.004	0.077	0.087	0.015	0.140	0.002	0.063
Ti	0.053	0.062	0.053	0.049	0.051	0.033	0.010	0.025	0.052	0.047	0.030	0.025	0.036	0.051	0.024	0.012
Al	4.581	3.787	4.581	6.201	4.583	4.683	5.363	4.491	5.835	5.524	5.704	6.046	5.707	4.476	5.822	5.899
Cr	10.077	9.626	10.077	8.407	9.129	9.977	9.380	9.813	8.469	8.821	8.414	8.084	8.855	9.619	8.609	8.154
Fe^{3+}	1.131	1.253	1.131	1.288	1.654	1.261	1.182	1.534	1.588	1.555	1.670	1.646	1.336	1.524	1.517	1.797
Fe^{2+}	4.631	4.216	4.631	3.731	4.157	4.278	4.128	4.385	3.749	3.896	4.083	3.641	3.998	4.835	4.019	3.807
Mn	0.125	0.086	0.125	0.095	0.100	0.099	0.121	0.099	0.093	0.101	0.112	0.106	0.109	0.105	0.086	0.088
Mg	3.274	4.332	3.274	4.188	3.990	3.642	3.701	3.577	4.188	4.022	3.860	4.311	3.907	3.185	3.872	4.053
Ca	0.029	0.021	0.029	0.000	0.014	0.000	0.007	0.019	0.009	0.009	0.004	0.042	0.036	0.043	0.008	0.090
Zn	0.046	0.013	0.046	0.037	0.057	0.021	0.080	0.000	0.015	0.022	0.047	0.013	0.000	0.023	0.041	0.038
Sum	24.00	24.00	24.00	24.00	24.00	24.00	24.00	24.00	24.00	24.00	24.00	24.00	24.00	24.00	24.00	24.00
Cr#	0.69	0.72	0.67	0.58	0.67	0.68	0.64	0.69	0.59	0.61	0.60	0.57	0.61	0.68	0.60	0.58
Fe^{3+}#	0.20	0.23	0.30	0.26	0.29	0.23	0.22	0.26	0.30	0.29	0.29	0.31	0.25	0.24	0.27	0.32
Mg#	0.41	0.51	0.41	0.53	0.49	0.46	0.47	0.45	0.53	0.51	0.49	0.54	0.49	0.40	0.49	0.52

Table 9. ...Continued

Sample	26-1a	26-1a	26-1a	26-1b	26-1b	26-1b	26-2a	26-2a	26-1a	26-1a	26-1b	26-1b	26-1b	26-2a	26-2a	26-2a
Analysis	1	2	3	1	3	4	2	5	4	5	2	5	6	1	3	4
Lithology	Metadunite															
Comment	Core								Rim							
SiO_2	0.00	0.23	0.06	0.11	0.03	0.04	0.01	0.02	0.13	0.04	0.03	0.04	0.02	0.00	0.04	0.07
TiO_2	0.10	0.09	0.08	0.16	0.13	0.15	0.11	0.19	0.10	0.14	0.03	0.15	0.12	0.16	0.11	0.11
Al_2O_3	14.87	15.12	15.00	13.89	16.05	15.99	15.01	10.15	16.16	15.35	15.32	15.99	15.60	14.00	14.78	13.15
Cr_2O_3	44.12	44.87	43.61	46.68	44.59	45.63	43.39	43.92	40.75	41.81	43.63	45.63	40.63	42.49	43.06	41.54
FeO*	33.48	33.34	33.89	32.67	30.37	30.72	33.28	35.46	35.42	36.13	31.67	34.73	36.31	33.72	33.84	34.13
MnO	0.54	0.59	0.62	0.60	0.44	0.48	0.48	0.73	0.41	0.77	0.49	0.72	0.56	0.47	0.41	0.38
MgO	6.40	6.58	6.34	6.78	7.65	7.68	8.09	5.79	6.35	5.46	7.21	6.10	6.06	7.79	7.56	6.12
CaO	0.05	0.02	0.04	0.02	0.00	0.01	0.03	0.03	0.03	0.00	0.01	0.02	0.00	0.01	0.02	0.05
ZnO	0.380	0.32	0.27	0.35	0.36	0.48	0.31	0.21	0.37	0.24	0.10	0.23	0.35	0.23	0.30	0.21
Total	99.93	101.15	99.89	101.27	99.617	101.19	101.28	96.55	99.71	99.95	98.49	103.61	99.65	98.86	100.13	95.83
	Oxygen#=32															
Si	0.001	0.059	0.016	0.029	0.007	0.011	0.004	0.004	0.033	0.012	0.007	0.011	0.005	0.005	0.009	0.020
Ti	0.020	0.018	0.016	0.032	0.026	0.029	0.021	0.040	0.019	0.029	0.007	0.029	0.024	0.024	0.022	0.023
Al	4.631	4.646	4.671	4.284	4.947	4.864	4.583	3.341	5.011	4.799	4.798	4.811	4.864	4.864	4.557	4.292
Cr	9.220	9.250	9.111	9.656	9.224	9.311	8.887	9.700	8.480	8.767	9.164	9.210	8.495	8.495	8.906	9.093
Fe^{3+}	2.108	1.949	2.152	1.939	1.764	1.743	2.481	2.870	2.404	2.353	2.009	1.898	2.583	2.583	2.473	2.529
Fe^{2+}	5.292	5.322	5.336	5.210	4.881	4.887	4.728	5.412	5.391	5.661	5.026	5.516	5.448	5.448	4.930	5.372
Mn	0.120	0.131	0.138	0.133	0.098	0.104	0.106	0.172	0.091	0.172	0.110	0.156	0.125	0.125	0.091	0.090
Mg	2.520	2.557	2.497	2.646	2.984	2.955	3.122	2.411	2.490	2.160	2.854	2.320	2.388	2.388	2.947	2.524
Ca	0.015	0.006	0.011	0.005	0.000	0.002	0.009	0.007	0.008	0.000	0.003	0.005	0.000	0.000	0.006	0.013
Zn	0.074	0.062	0.052	0.068	0.070	0.091	0.059	0.042	0.072	0.047	0.020	0.043	0.068	0.068	0.058	0.043
Sum	24.00	24.00	24.00	24.00	24.00	24.00	24.00	24.00	24.00	24.00	24.00	24.00	24.00	24.00	24.00	24.00
Cr#	0.67	0.67	0.66	0.69	0.65	0.66	0.66	0.74	0.63	0.65	0.66	0.64	0.67	0.67	0.66	0.68
Fe^{3+}#	0.31	0.30	0.32	0.29	0.26	0.26	0.34	0.35	0.32	0.33	0.30	0.28	0.35	0.35	0.33	0.32
Mg#	0.32	0.33	0.32	0.34	0.38	0.38	0.40	0.31	0.32	0.28	0.36	0.30	0.31	0.32	0.37	0.32

their metamorphic origin.

Forsterite content of the analyzed metamorphic olivines is similar to the composition of metamorphic olivines reported from the metamorphosed mantle peridotites (e.g., Springer, 1974; Arai, 1975; Pinsent and Hirst, 1977; Nozaka, 2018). Therefore, the mantle peridotites should be the protolith of the studied metaperidotites. The NiO (wt%) versus Fo (mole%) contents of olivines graph (Figure 8A; Nozaka, 2010) shows that the analyzed olivines have metamorphic nature. The NiO against Fo binary diagram (Figure 8B) shows that the olivines of the studied metaperidotites are similar to the metamorphic olivines with magnetite inclusions from Braszowice - Brzeźnica serpentinites (SW Poland; Wojtulek et al., 2017). The forsterite content of olivines and their variable MnO contents reveal that these samples are of the deserpentinized peridotites (Guotana et al., 2018; Figure 8C).

Metamorphic orthopyroxene forms at the expense of olivine, anthophyllite and talc at temperatures above

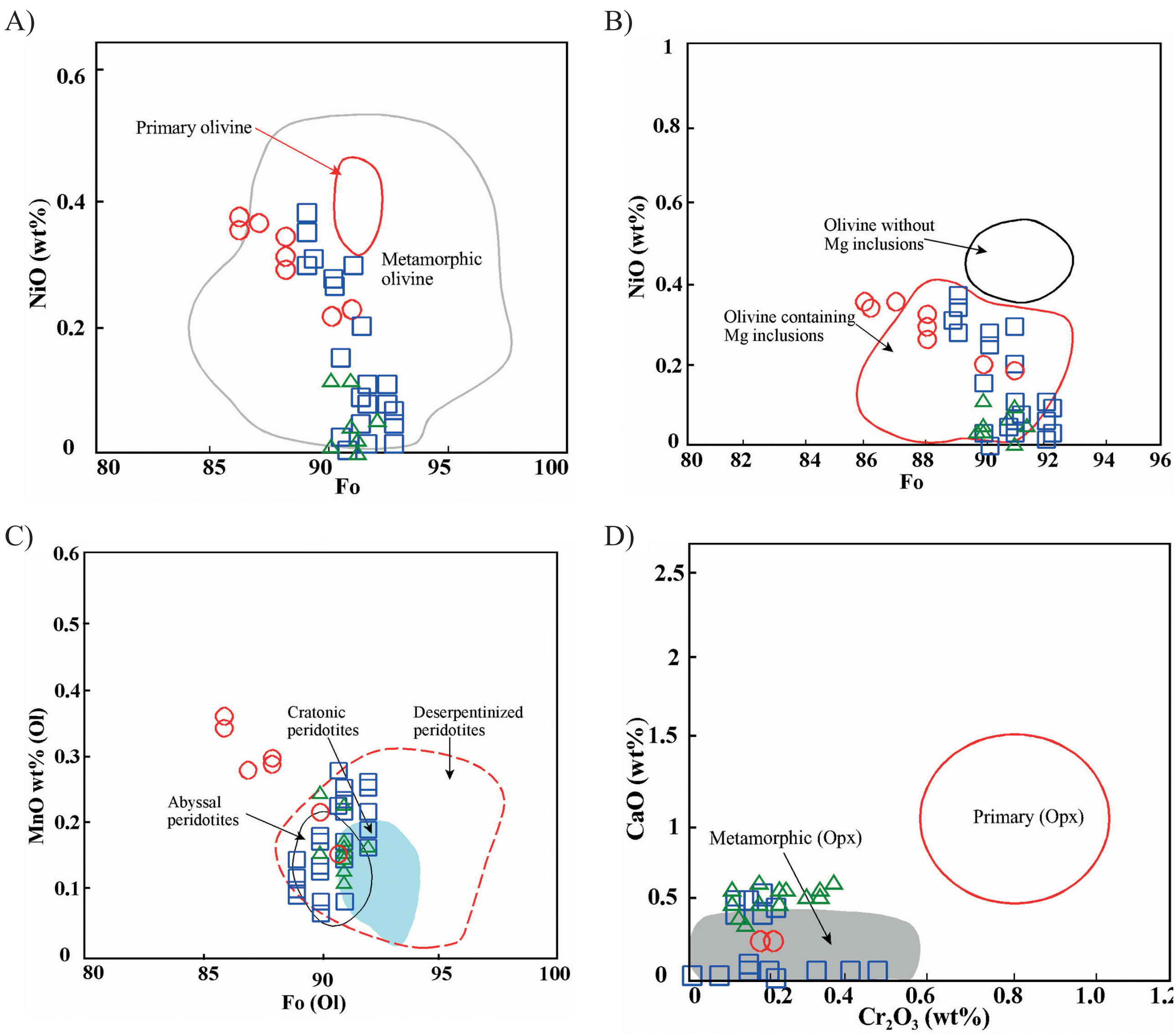

Figure 8. (A and B) NiO (wt%) against Fo (mole.%) content graph of olivines (Nozaka, 2005; Wojtulek et al., 2017; respectively); (C) Forsterite content versus MnO values (wt%) plot of olivines (Guotana et al., 2018). Compositions of metamorphic olivines from the Happo-O'ne peridotite complex (Khedr and Arai, 2012), Tari-Misaka (Arai, 1975), Ohsa-Yama (Nozaka, 1995) in Japan, and abyssal peridotites (Warren, 2016) are also included for comparison. (D) CaO values Cr_2O_3 contents diagram (The field of metamorphic orthopyroxene is from Pinsent and Hirst ,1977; Desmarais, 1981; Tracy et al. 1984; Nozaka, 2010, samples).The fields of residual and melt impregnation clinopyroxenes are from Seyler et al. (2007).

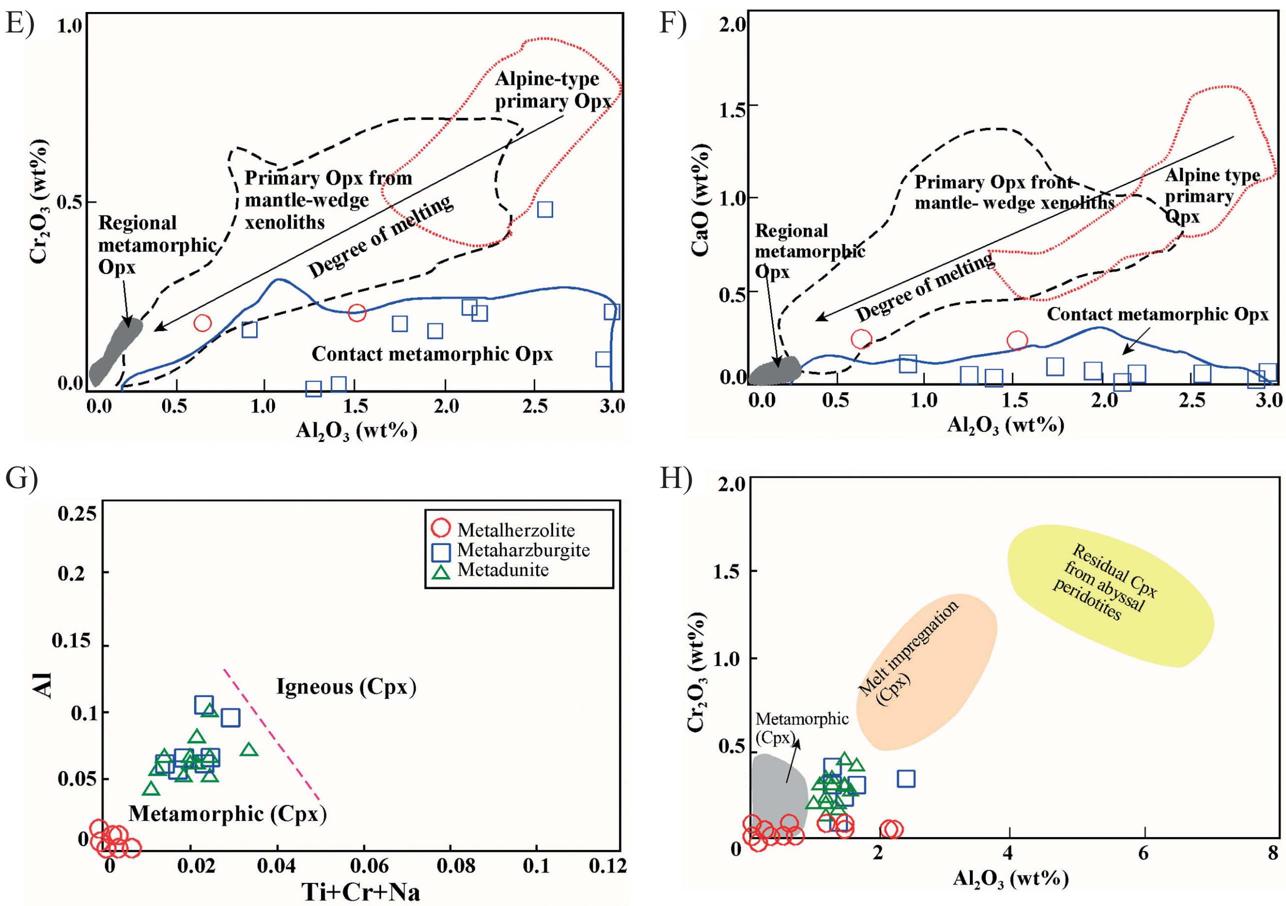

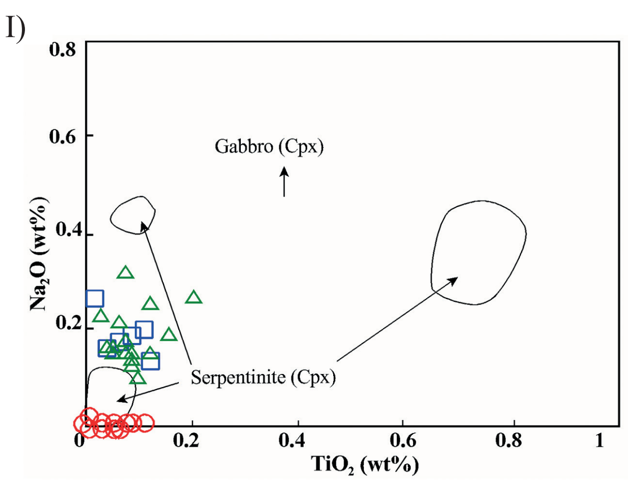

Figure 8. Continued. (E and F) Cr_2O_3 values Al_2O_3 and CaO against Al_2O_3 graphs (Frost, 1975). Fields of contact metamorphic orthopyroxene are from Arai (1975); Pinsent and Hirst (1977). (G) Diagram to distinguish the igneous and metamorphic clinopyroxene (Veblen and Ribbe, 1982). (H) Cr_2O_3 values Al_2O_3 (wt%) diagram. The fields of residual and melt impregnation clinopyroxenes are from Seyler et al. (2007). The field of metamorphic clinopyroxene is from Nozaka and Shibata (1995). (I) Na_2O values TiO_2 (wt%) diagram (Wojtulek et al., 2017).

700 °C (Spear, 1995; Pawley, 1998). This mineral is formed according to the reactions:

$$\text{Talc} + \text{Forsterite} \rightarrow \text{Enstatite} + H_2O \quad (4)$$

$$\text{Anthopyllite} + \text{Forsterite} \rightarrow \text{Enstatite} + H_2O \quad (5)$$

The low CaO content of orthopyroxenes is a prominent feature of the metamorphic orthopyroxenes (Nozaka, 2010). The CaO and Cr_2O_3 values of the studied orthopyroxenes (average of 0.27 and 0.26, respectively) are in range of those formed from low-grade metamorphism of peridotites (Nozaka, 2010) and are also similar to the reported metamorphic orthopyroxenes from the Jandaq metaultrabasic rocks in Central Iran (Torabi et al., 2011a). The CaO (wt%) against Cr_2O_3 (wt%) content diagram (The field of metamorphic orthopyroxene is from Pinsent and Hirst, 1977; Desmarais, 1981; Tacy et al., 1984; Nozaka, 2010, samples) used to identify the type of orthopyroxenes (Figure 8D). Chemical composition of the studied orthopyroxenes reveal that they are similar to the metamorphic orthopyroxenes. In the Cr_2O_3 against Al_2O_3 and CaO versus Al_2O_3 graphs (Frost, 1975; Figure 8 E,F), orthopyroxenes of the Kal-e-Kafi area metaperidotites are plotted in the field of orthopyroxenes with contact metamorphism nature.

The low amounts of CaO (0 to 0.6 wt%; average: 0.27 wt%) and the wollastonite endmember contents (0 to 1.12%; average: 0.54%) of these orthopyroxenes indicate that they are similar to the “Non-calciferous” orthopyroxenes which are produced by thermal metamorphism of strongly serpentinized peridotites by intrusion of granitic masses (Arai, 1974).

The average content of Na_2O in clinopyroxenes of the Kal-e-Kafi metaperidotites is 0.01 wt%, therefore, can not be considered as primary clinopyroxenes (e.g., Khedr and Arai, 2012). In the (Ti+Na+Cr) versus Al (Berger et al., 2005; Figure 8G) and Cr_2O_3 against Al_2O_3 (Seyler et al., 2007, Nozaka and Shibata, 1995; Figure 8H) diagrams, the studied clinopyroxenes plotted in the field of clinopyroxenes with metamorphic nature. The Na_2O against TiO_2 graph of the metamorphic clinopyroxenes (Wojtulek et al., 2017) (Figure 8I), shows that the studied clinopyroxenes are nearly similar to the clinopyroxenes from serpentinites.

The chondrite-normalized REE patterns (REE values of chondrite are from Sun and McDonough, 1989) of the clinopyroxenes in the Kal-e-Kafi area metaperidotites (Figure 9) indicate that there two types of clinopyroxenes in these rocks. (1) Clinopyroxenes of metalherzolites are enriched in light rare earth elements (LREE) and exhibit a nearly flat heavy rare earth elements (HREE) patterns. (2) On the other hand, clinopyroxenes of the metaharzburgites exhibit a flat and almost depleted patterns for LREE and HREE. The REE patterns of the studied clinopyroxenes are different from clinopyroxenes of supra-subduction zones (SSZ) (Bizimis et al., 2000) and abyssal peridotites (Johnson and Dick, 1992; Warren and Shimizu, 2010), likely due to their metamorphic nature.

The primitive mantle-normalized multi-elements spider diagram (McDonough and Sun, 1995) of the studied clinopyroxenes (Figure 9) indicate that clinopyroxenes of metalherzolites have higher values of the most of trace elements than the clinopyroxenes of metaharzburgites. Clinopyroxenes of metaharzburgites are enriched only in U and Pb and for other elements show depletion (<1) (Figure 9).

The chondrite-normalized REE patterns and primitive mantle-normalized spidergram of the studied clinopyroxenes (Figure 9) indicate that trace element concentrations of clinopyroxenes from metalherzolites exhibit more variations than the clinopyroxenes of metaharzburgites and HREE contents of both clinopyroxenes are transitional between chemical composition of clinopyroxenes from supra-subduction zones (SSZ) (Bizimis et al., 2000) and abyssal peridotites (Johnson and Dick, 1992; Warren and Shimizu, 2010).

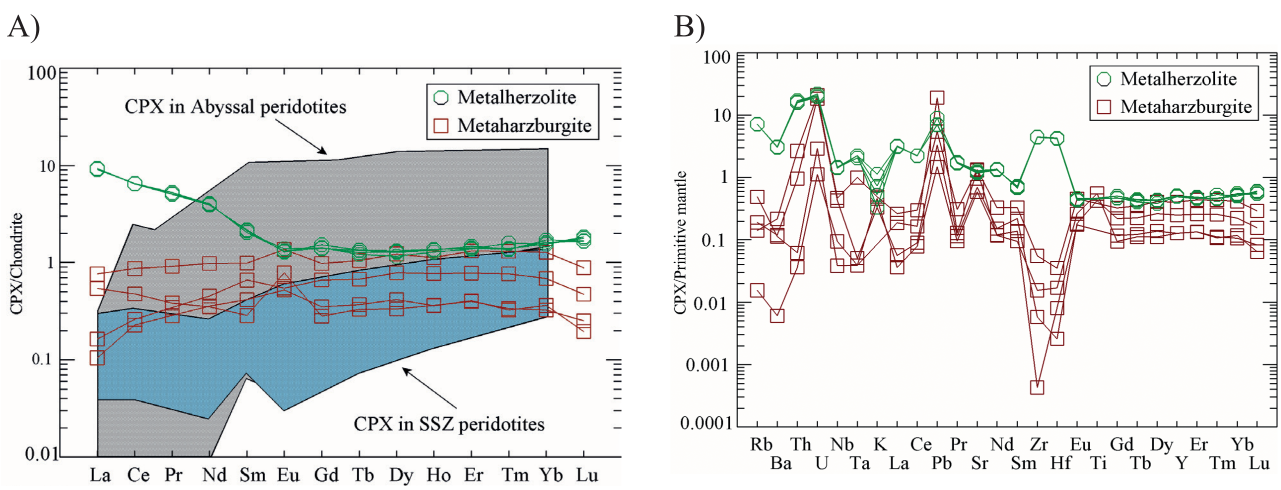

Figure 9. (A) Chondrite-normalized REE patterns and (B) Primitive mantle-normalized multi-elements spidergram of clinopyroxenes from the Kal-e-Kafi metaperidotites. Normalizing values of chondrite and primitive mantle are from Sun and McDonough (1989) and McDonough and Sun (1995). The field of clinopyroxenes in abyssal-peridotites and supa-subduction zone peridotites are from Johnson and Dick, 1992; Warren and Shimizu, 2010 and Bizimis et al., 2000, respectively.

Table 10. Geochemical compositions of clinopyroxenes in metaperidotites of the Kal-e-Kafi area (Major elements in wt% by EPMA and trace elements in ppm by LA-ICP-MS).

Sample	B809	B809	B809	B809	B807	B807	B807	B807
Analysis	201	202	206	208	191	192	195	196
Lithology	Metaharzburgite				Metalherzolite			
SiO_2	55.17	54.77	54.98	55.85	56.07	56.20	56.07	56.11
TiO_2	0.09	0.12	0.00	0.00	0.00	0.00	0.00	0.00
Al_2O_3	1.44	2.08	1.10	0.65	0.05	0.03	0.10	0.05
Cr_2O_3	0.02	0.01	0.06	0.00	0.00	0.00	0.00	0.06
FeO*	1.91	1.92	1.88	1.73	1.45	0.94	0.95	0.91
MnO	0.08	0.08	0.04	0.05	0.09	0.08	0.08	0.08
MgO	16.66	16.59	16.99	17.09	17.35	17.64	17.63	17.60
CaO	24.96	24.67	25.05	24.80	24.74	24.90	24.93	24.83
Na_2O	0.01	0.01	0.00	0.00	0.01	0.00	0.02	0.00
K_2O	0.01	0.00	0.01	0.01	0.02	0.01	0.03	0.02
NiO	0.03	0.04	0.04	0.02	0.03	0.04	0.00	0.01
Total	100.38	100.29	100.17	100.20	99.82	99.85	99.81	99.67
Li	20.088	11.107	12.022	7.479	3.433	3.982	3.396	4.334
Rb	0.121	0.314	0.010	0.089	4.532	4.531	4.531	4.553
Sr	14.759	27.528	12.456	28.395	27.205	24.712	25.288	25.972
Y	1.139	0.584	0.583	1.847	2.306	2.256	2.291	2.339
Zr	0.065	0.175	0.005	0.624	49.793	49.971	50.514	50.536
Nb	0.305	0.028	0.067	0.335	1.018	1.044	1.011	1.029
Ba	0.832	0.793	0.043	1.520	21.728	21.660	21.818	21.252
La	0.039	0.129	0.025	0.181	2.191	2.153	2.191	2.203
Ce	0.160	0.293	0.140	0.532	3.983	3.988	3.992	3.955
Pr	0.032	0.036	0.026	0.085	0.488	0.470	0.474	0.468
Nd	0.207	0.161	0.163	0.448	1.835	1.800	1.853	1.787
Sm	0.098	0.042	0.062	0.147	0.303	0.316	0.302	0.323
Eu	0.031	0.044	0.029	0.077	0.074	0.073	0.078	0.072
Gd	0.132	0.056	0.070	0.195	0.277	0.283	0.280	0.303
Tb	0.024	0.012	0.013	0.038	0.048	0.044	0.046	0.048
Dy	0.193	0.082	0.102	0.303	0.314	0.286	0.318	0.324
Ho	0.042	0.020	0.020	0.061	0.074	0.070	0.074	0.074
Er	0.124	0.064	0.065	0.210	0.235	0.220	0.223	0.226
Tm	0.019	0.008	0.008	0.032	0.034	0.039	0.034	0.034
Yb	0.110	0.053	0.058	0.206	0.262	0.249	0.274	0.251
Lu	0.012	0.006	0.005	0.022	0.041	0.045	0.041	0.044
Hf	0.001	0.005	0.002	0.011	1.315	1.298	1.337	1.309
Ta	0.002	0.002	0.002	0.041	0.092	0.092	0.092	0.085
Pb	0.619	3.510	0.273	1.011	1.297	1.307	1.283	1.675
Th	0.081	0.005	0.003	0.227	1.345	1.384	1.458	1.361
U	0.386	0.061	0.024	0.437	0.411	0.432	0.433	0.459

Some clinopyroxenes from metaharzburgites show a slight depletion in La, Ce and Pr relative to Nd (Figure 9A).

The LREE-enriched shapes of clinopyroxenes from metalherzolites of the Kal-e-Kafi area (Figure 9A) can be attributed to the metasomatic enrichment events (Beccaluva et al., 2001), which probably imposed by the Eocene pluton and thermal metamorphism.

The calc-alkaline nature of the Eocene pluton (Salim et al., 2018), as well as probably partially carbonation of the host serpentinized peridotites (formation of listwaenites) (Salim et al., 2018) and presence of tremolite can be the sources of Calcium for crystallization of metamorphic clinopyroxene. This calc-alkaline magma was rich in fluids (subduction-related magma) and it's interaction with the country rocks formed contact metamorphism as skarn, hornfels and metaperidotites.

According to petrography evidences, tremolites are observed in two types of prismatic and acicular crystals (Scotford and Williams, 1983). Prismatic tremolites present poikiloblastic texture with magnetite and chlorite inclusions. Acicular tremolites show nematoblastic and jack-straw textures and have intergrowth with olivine and serpentine minerals. The margins of some tremolites are replaced by chlorite which points to the retrograde metamorphism after progressive metamorphism (Evans, 1977; Torabi et al., 2011a). Tremolites are formed at the expense of clinopyroxene according to the reaction:

Diopside + Antigorite → Forsterite + Tremolite + H_2O (6)

The Na content of amphiboles in the host rock controls by the temperature of the intrusive body (Frost, 1975). Wide chemical composition ranges of calcic amphiboles in the studied metaperidotites from tremolite to hornblende, tschermachite, anthopyllite and gedrite (Figures 7E and F) possibly corresponds to the intrusion of the Kal-e-Kafi pluton. Moreover, the extensive variations in MnO content of the olivines (0.6-0.36 wt%) and the high Al_2O_3 value of chlorites (18-20 wt%) in the studied rocks can be attributed to the interactions of metaperidotites with the Kal-e-Kafi Eocene pluton. According to the low value of Ti (<0.08 apfu) in these amphiboles, it is concluded that all amphiboles in the studied metalherzolites have metamorphic nature (Leake, 1965; Figure 10A). In the Na versus Si diagram, most of the amphiboles are plotted long the prograde metamorphism trend (Figure 10B) (Fields are from Frost, 1975; Pinsent and Hirst, 1977; Nozaka, 2005).

Anthophyllites probably have formed by the reactions of talc+olivine and talc+orthopyroxene at temperatures between 600 to 700 °C and pressures less than 12 kbar (Spear, 1995). These minerals are formed according to the reactions:

Talc + Forsterite → Anthophyllite + H_2O (7)
Talc + Enstatite → Anthophyllite (8)

According to the petrography evidences, mineral chemistry and XRD patterns, the studied serpentine minerals are largely identified as antigorite (Figure 6). The antigorite is stable up to ~800°C (Gualtieri et al., 2012). They probably broken down to forsterite and talc by increasing the metamorphic grade. Lizardite is also observed in margin of some olivine neoblasts and fills the fractures (Figures 5 A,E,F). Lizardite is product of the retrograde metamorphism process and serpentinization of olivines (M3). Chrysotile breaks down to talc and forsterite, and antigorite breaks down to talc, forsterite and chlorite during high grade metamorphism (Spear, 1995; Bucher and Grapes, 2011). These reveals that the talc, olivine and Mg-chlorite in the studied rocks are formed during the progressive metamorphism.

Chlorite content of the metalherzolites is higher than the metaharzburgites. Mg-chlorite in metaperidotites (Mg-rich rocks) is stable at temperatures higher than the 720 °C (Spear, 1995).

According to the petrography characteristics, primary Cr-spinels break down to magnetite and chromian magnetite by increasing the degree of metamorphism (Evans and Frost, 1975; Frost, 1975; Barnes and Roeder, 2001; Mellini et al., 2005; 2009) through the following reaction:

Al-Spinel + Serpentine + H_2O + O_2 → Chlorite + Cr-Magnetite (9)

The presence of Mg-chlorite, chromian magnetite and magnetite in the studied metaperidotites point to the metamorphism at about 720 °C.

The metaharzburgites are found in the contact of the Eocene pluton, therefore, their plagioclases probably are formed by the Eocene magma. These plagioclases (An_{91-94}) are chemically similar to the plagioclases from the gabbros in the Eocene Kal-e-Kafi pluton (An_{84-94}) (Average: 91.6%) (Salim, 2019 and Salim et al., 2018) (Figure 7H).

The Cr-spinel is the only primary mineral that may preserve its original chemical composition even in completely serpentinized peridotites and can show chemical zoning from the core to rim, whereas the other primary minerals (olivines and pyroxenes) may completely alter to serpentine (Arai et al., 2006). According to Evans and Frost (1975), the Cr content of spinels increases with increasing the grade of metamorphism up to the middle amphibolite facies conditions. Increasing the Cr# content may be occurred due to the reactions between Cr-spinels and chlorite from host rocks (Colas et al., 2014, Gervilla

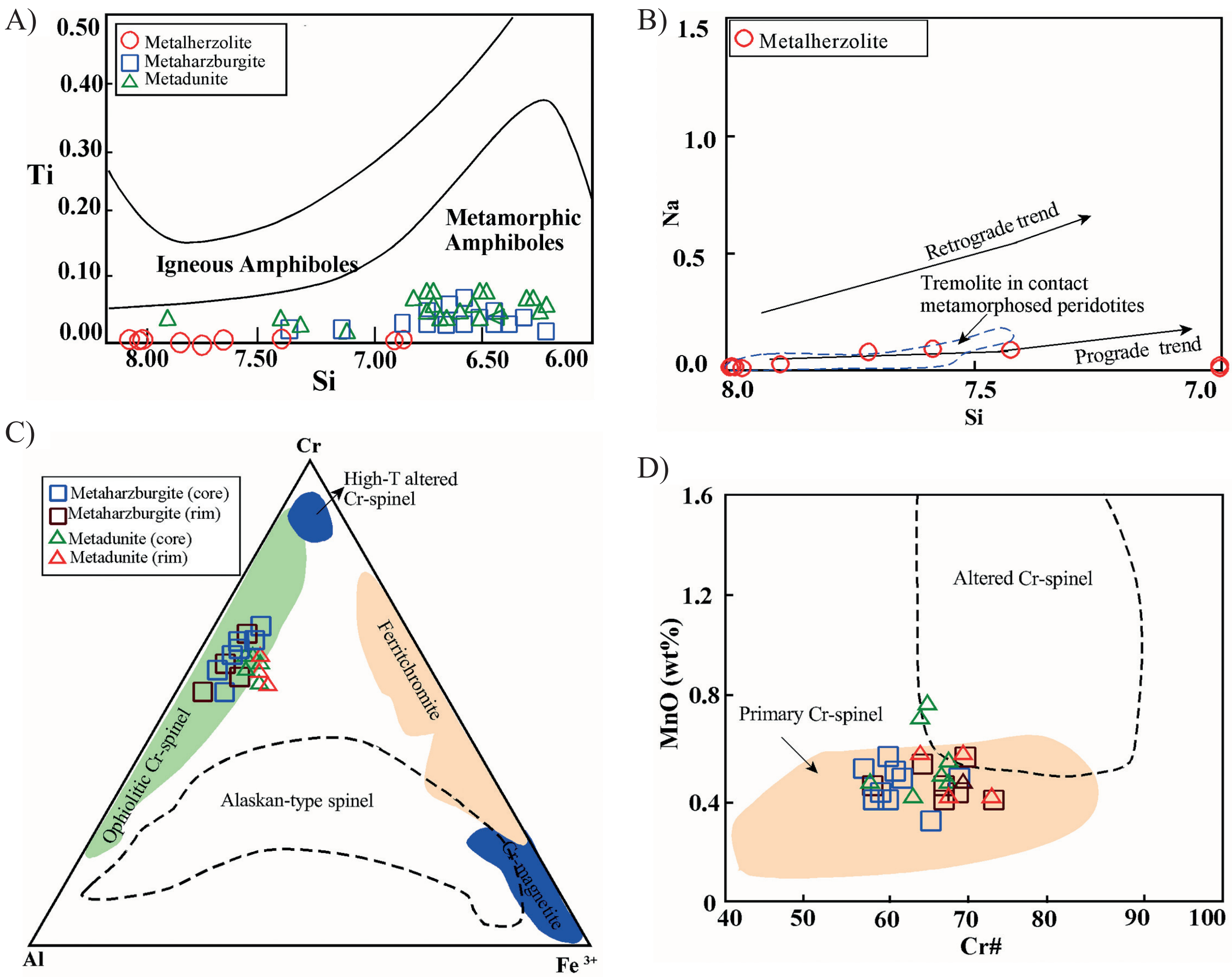

Figure 10. (A) Diagram to identify the nature of amphiboles (Leake, 1965); (B) Na values against Si diagram, tremolites field of contact metamorphism is from Frost (1975); Pinsent and Hirst (1977); Nozaka, (2005). (C) Compositional variations of Cr-spinels from the Kal-e-Kafi metaperidotites in ternary plot of the Cr–Al–Fe^{3+} atomic ratio. Compositional fields of ophiolitic Cr-spinel, Cr-magnetite and ferritchromite are from Barnes and Roeder (2001), the field of Alaskan-type spinels is from Ahmed and Hariri (2008) and Abdel Halim et al. (2016); and the high-T altered spinel field is from Arai et al. (2006). (D) MnO against Cr# diagram (after Khedr and Arai, 2017).

et al., 2012). Mineral assemblages and chemistry of the Cr-spinels in the studied metaperidotites form the Kal-e-Kafi area indicate that they are similar to the Cr-spinels which formed as a result of the contact metamorphism by a granitic intrusion (e.g., Ahmed and Surour, 2016).

Using the Al^{3+}-Cr^{3+}-Fe^{3+} ternary diagram to show the chemical position of Cr-spinels (Ahmed et al., 2016) indicate their ophiolitic Cr-spinel composition (Figure 10C). In the MnO (wt%) versus Cr# diagram (Figure 10D; after Khedr and Arai, 2012), and Cr# against Mg# (Figure 10E; Merlini et al., 2009; Grieco and Merlini, 2012) graph all the spinels are plotted in the primary Cr-spinel field.

The Cr_2O_3 content of Cr-spinels from the metaperidotites (42.37 to 47.69 wt %) attest that they originated from a depleted to moderately depleted mantle source (e.g., Dick and Bullen, 1984; Conrad and Kay 1984; Haggerty, 1988; Kepezhinskas, et al., 1995; Kamenetsky et al., 2001; Figure 10F), belonging to the SSZ peridotites (Juteau and Maury, 1999; Figure 10G).

According to OSMA plot diagram (Arai, 1994; Figure 10H), the partial melting of the studied metaperidotites has taken place at about 30% in a supra-subduction zone (SSZ) or a back-arc basin environment.

According to the above mentioned paragraphs, the minerals of these metaperidotites can be classified as primary (core of some Cr-spinels), metamorphic

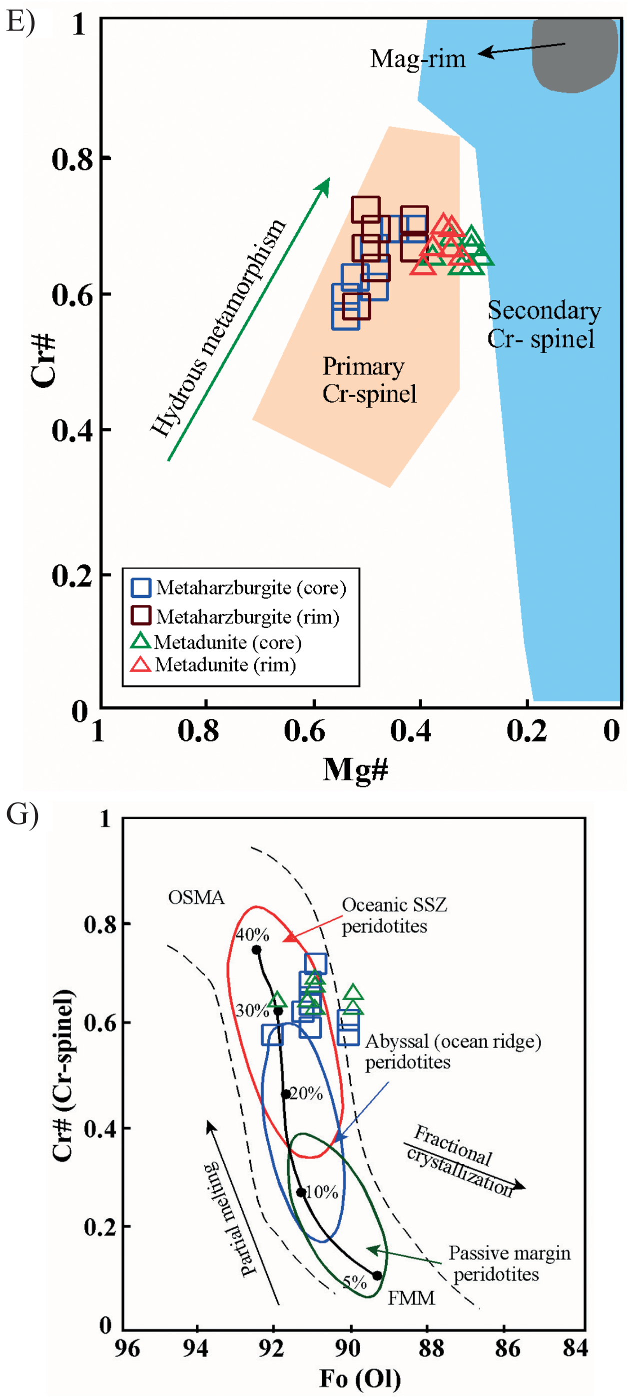

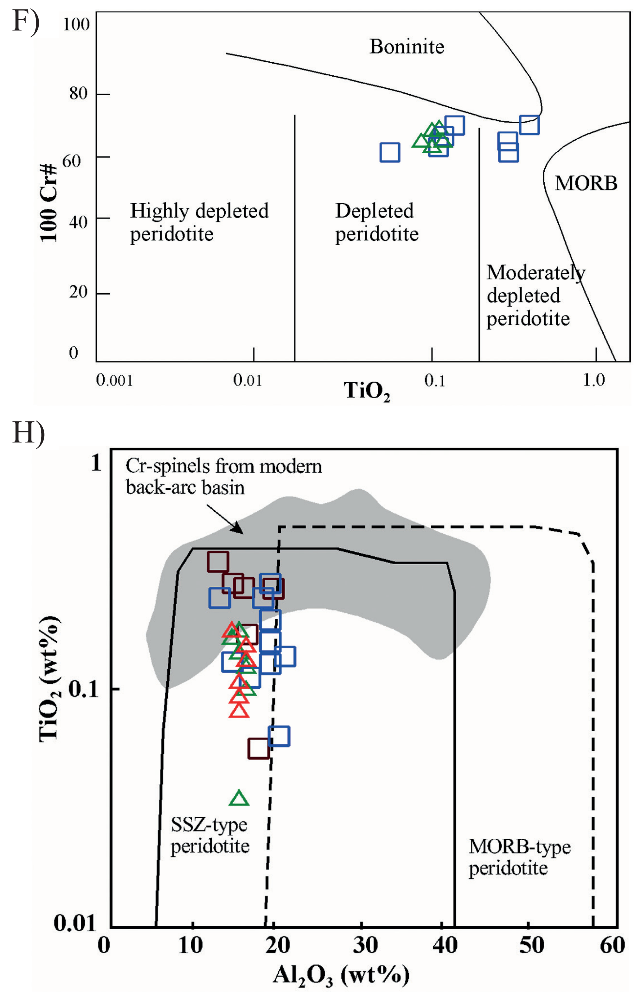

Figure 10. Continued. (E) Mg# versus Cr# diagram (Merlini et al., 2009; Grieco and Merlini, 2012) of Cr-spinels from the Kal-e-Kafi metaperidotites. (F) TiO_2 against Cr# binary plot (after (Juteau and Maury, 1999). (G) Fo (Ol) against Cr# (Sp) diagram. Olivine-spinel mantle array (OSMA) and melting trends with fertile mantle MORB (FMM) are from Arai (1994). The passive margin, abyssal and supra-subduction zone (SSZ) peridotites are from Dick and Bullen (1984), Parkinson and Pearce (1998), Pearce et al. (2000) and Choi et al. (2008). (H) Al_2O_3 against TiO_2 in spinels tectonic discrimination diagram (fields of SSZ and MOR peridotites, as well as the spinels from modern back-arc basin, are adopted from Kamenetsky et al. (2001).

(olivine, orthopyroxene, clinopyroxene, talc, hornblende, antophyllite, Mg-chlorite and acicular tremolite) and late alteration (lizardite, chlorite in the margin of some tremolites).

THE P-T CONDITION OF METAMORPHISM

Metaperidotites

There is no thermobarometer suggested for P-T estimation of metamorphism of ultramafic rocks. Therefore, Bucher and Frey (1994) suggested the microscopic evidence, phase relationships and reactions involving volatile components (e.g., H_2O) to determine the P-T conditions of metamorphism in metaperidotites. However, since our observation confirm that the Kal-e-Kafi pluton was responsible for progressive metamorphism of the metapridotites, and the average crystallization temperature at 745 °C (Salim, 2019). Therefore, this metamorphic event has been occured at temperatures below 745 °C.

Petrography evidences that indicate occurrence of a progressive metamorphism in the studied metaperidotites are as follows:

1- The mineral assemblages of tremolite+olivine in metalherzolites and olivine+orthopyroxene+anthophyllite in metaharzburgites indicate a metamorphic event at temperatures up to 700 °C (Evans, 1977, Spear, 1995).

2- High abundances of tremolite and antigorite in the studied matalherzolites, absence of quartz, as well as the presence of talc in the metaharzburgites show that temperature of metamorphism probably is less than 800 °C and hence, peak metamorphism conditions never exceeded the related reactions (Desmarais, 1981; Giacobbe et al., 2012; Gualtieri et al., 2012). Tremolite is the main Ca-bearing mineral and is stable at temperatures above 650 °C (Bucher and Frey, 1994), which will decompose to diopside and enstatite by increasing metamorphic grade to above 800 °C.

3- The presence of Mg-chlorite and absence of Al-spinel in the studied metaperidotites, indicate that the temperature of metamorphism was below 720 °C (Forst, 1975; Sanford, 1982, Tracy et al., 1984). As the maximum stability limit for Mg-chlorite is ~720 °C and by increasing the metamorphic grade, chlorites will break down to Fo + En + Al-spinel (Bucher and Grapes, 2011).

4- The absence of green spinel (Al-rich) in the studied metaperidotites indicates that the temperature of prograde metamorphism was less than 750 °C (Dymek et al., 1988).

5- According to the following reaction, formation of orthopyroxenes in the studied metaperidotites possibly indicates that the temperature of metamorphism should be more than 700 °C (CMSH system Spear (1995):

$$\text{Tremolite} + \text{Olivine} = \text{Orthopyroxene} + H_2O \qquad (10)$$

6- High amount of antigorite in the studied rocks and its stability point to the temperatures less than 750 °C (Swartz et al., 2013).

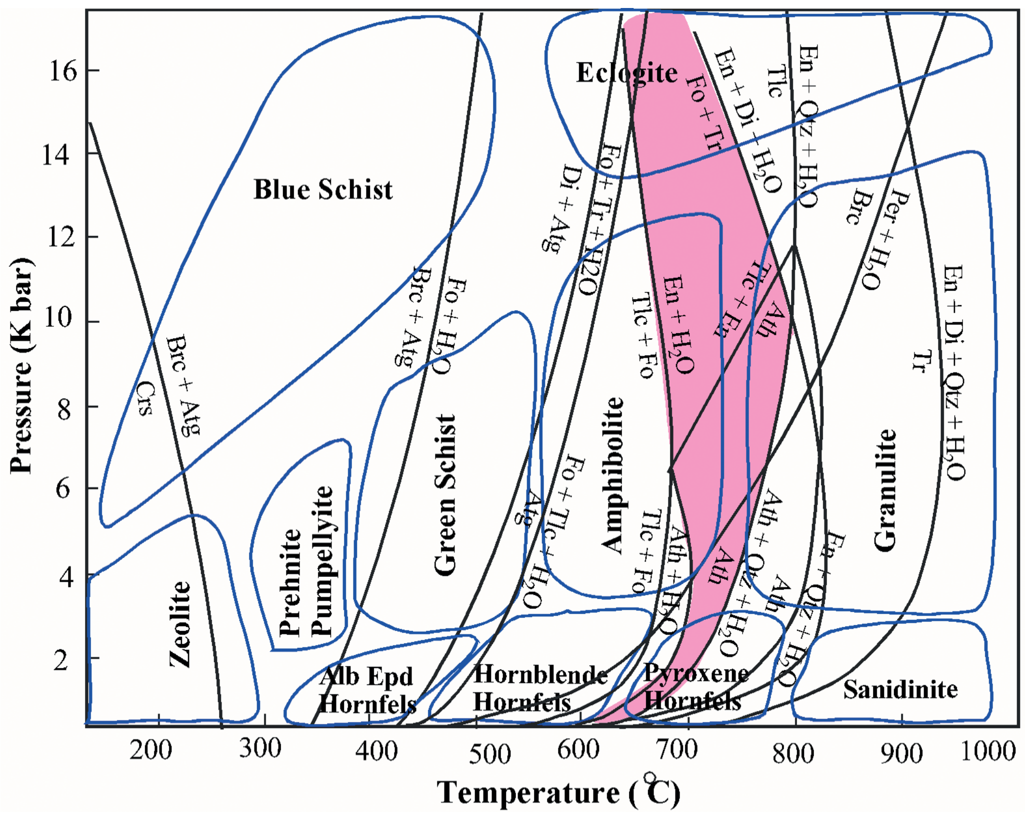

Figure 11. Combination of the P-T condition of metamorphism and metamorphic facies (Yardley, 1989) and graph of petrogenetic grid for water-saturated ultramafic rocks in the system $CaO\text{-}MgO\text{-}SiO_2\text{-}H_2O$ (CMSH) calculated from the thermodynamic data base of Spear (1995). The shaded field represents the P-T condition of peak metamorphism in the Kal-e-Kafi peridotites, deduced from the observed mineral assemblages.

Antigorite = Talc + Forsterite + H_2O (11)

7- The presence of anthophyllite crystals in the studied metaperdotites likely corresponds with a long duration of the thermal supply to the system (e.g., Nozaka, 2011).

8- The olivine+orthopyroxene±tremolite mineral paragenesis indicates that the maximum temperature of thermal metamorphism reachs up to approximately 750 °C (Fujimaki and Yomogida, 1986a and b).

9- Using the phase relationships of the CMSH (C = CaO, M = MgO, S = SiO_2, H = H_2O) system, which are designed based on the mineral assemblages and reactions that occur in ultramafic rocks (Spear, 1995), suggest the temperature range of 630 to 720 °C for contact metamorphism of the studied metaperidotites (Figure 11).

CONCLUSIONS

Intrusion of the Eocene age Kal-e-Kafi pluton caused the thermal metamorphism (characterized by olivine, orthopyroxene, clinopyroxene, tremolite, Mg-anthophyllite, serpentine, talc and chlorite) in the host metaperidotites. The presence of magnetite inclusions in metamorphic olivines and associated rock types (regionally metamorphosed Paleozoic schist and marble) indicate that the Kal-e-Kafi metaperidotites were partly metamorphosed in the greenschist facies at the Paleozoic (M1) before being progressively metamorphosed in pyroxene hornfels facies P-T condition in Eocene (M2). A late-stage retrograde metamorphism in greenschist facies (M3) caused to the chlorite and lizardite formation (M3) by partial replacement of tremolite, and serpentinization of some metamorphic olivines and orthopyroxenes, respectively.

Chemical characteristics of inner parts of Cr-spinels show that the Kal-e-Kafi metaperidotites possibly derived from depleted to moderately depleted mantle rocks which passed about 30% partial melting in a supra subduction zone environment.

ACKNOWLEDGEMENTS

The authors gratefully acknowledge the University of Isfahan (Iran), Kanazawa and Yamagata Universities (Japan) for financial support and providing laboratory facilities. We are also thank the reviewers for useful and constructive comments to important improvements in the manuscript.

REFERENCES

Abdel Halim A.H., Helmy H.M., Abd El-Rahman Y.M., Shibata T., El Mahallawi M.M., Yoshikawa M., Arai S., 2016. Petrology of the Motaghairat mafic-ultramafic complex, Eastern Desert, Egypt: a high-Mg post-collisional extension-related layered intrusion. Journal of Asian Earth Sciences 116, 164-180.

Ahmadian J., Sarjoughian F., Lentz D., Esna-Ashari A., Murata M., Ozawa H., 2016. Eocene K-rich adakitic rocks in the Central Iran: Implications for evaluating its Cu–Au–Mo metallogenic potential. Ore Geology Reviews 72, 323-342.

Ahmed Z. and Hariri M.M., 2008. Neoproterozoic ophiolites as developed in Saudi Arabia and their oceanic and pericontinental domains. Arabian Journal for Science and Engineering 33, 17-54.

Ahmed A.H. and Surour A.A., 2016. Fluid-related modifications of Cr-spinel and olivine from ophiolitic peridotites by contact metamorphism of granitic intrusions in the Ablah area, Saudi Arabia. Journal of Asian Earth Sciences 122, 58-79.

Aistov L., Melnikov B., Krivyakin B., Morozov L., 1984. Geology of the Khur Area (Central Iran). Geological Survey of Iran, V/O “Technoexport”, Report TE/No. 20, 132 pp.

Arai S., 1974. “Non-calciferous” orthopyroxene and its bearing on the petrogenesis of ultramafic rocks in Sangun and Joetsu zones. The Journal of the Japanese Association of Mineralogists, Petrologists and Economic Geologists 69, 343-353.

Arai S., 1975. Contact metamorphosed dunite-harzburgite complex in the Chugoku district, western Japan. Contributions to Mineralogy and Petrology 52, 1-16.

Arai S., 1994. Characterization of spinel peridotites by olivine-spinel compositional relationships: review and interpretation. Chemical Geology 113, 191-204.

Arai S., Shimizu Y., Ismail S.A., Ahmad A.H., 2006. Low-T formation of high-Cr spinel with apparently primary chemical characteristics within podiform chromitite from Rayat, northeastern Iraq. Mineralogical Magazine 70, 499-508.

Bagheri S., 2007. The exotic Paleo-Tethys terrane in Central Iran: new geological data from Anarak, Jandaq and Posht-e-Badam areas. Ph.D. Thesis, Lausanne University, Switzerland, 208 pp.

Bagheri S. and Stampfli G.M., 2008. The Anarak, Jandaq and Posht-e-Badam metamorphic complex in central Iran: New geological data, relationships and tectonic implications. Tectonophysics 451, 123-155.

Barnes S.J. and Roeder P.L., 2001. The range of spinel compositions in terrestrial mafic and ultramafic rocks. Journal of Petrology 12, 2279-2302.

Beccaluva L., Bonadiman C., Coltorti M., Salvini L., Siena F., 2001. Depletion events, nature of metasomatizing agent and timing of enrichment processes in lithospheric mantle xenoliths from the Veneto volcanic province. Journal of Petrology 42, 173-187.

Berger J., Femenias O., Mercier J.C.C., Demaiffe D., 2005. Ocean-floor hydrothermal metamorphism in the Limousin ophiolites (western French Massif Central): evidence of a rare preserved Variscan oceanic marker. Journal of Metamorphic Geology 23, 795-812.

Bizimis M., Salters V.J.M., Bonatti E., 2000. Trace and REE content of clinopyroxenes from supra-subduction zone peridotites. Implications for melting and enrichment processes in island arcs. Chemical Geology 165, 67-85.

Bucher K. and Frey M., 1994. Petrogenesis of metamorphic rocks. Springer, Berlin, 318 pp.

Bucher K. and Grapes R., 2011. Petrogenesis of metamorphic rocks. Springer, Berlin, 428 pp.

Choi S.H., Shervais J.W., Mukasa S.B., 2008. Supra-subduction and abyssal mantle peridotites of the coast range ophiolite, California. Contributions to Mineralogy and Petrology 156, 551-576.

Colas V., Gonzalez-Jimenez J.M., Griffin W.L., Fanlo I., Gervilla F., O'Reilly S.Y., Pearson, N.J., Kerestedjian T., Proenza J.A., 2014. Fingerprints of metamorphism in chromite: New insights from minor and trace elements. Chemical Geology 389, 137-152.

Coleman R.G., 1977. Ophiolites: Ancient oceanic lithosphere. Springer, Berlin, 229 pp.

Conrad W.K. and Kay R.W., 1984. Ultramafic and mafic inclusions from Adak Island: crystallization history and implications for the nature of primary magmas and crustal evolution in the Aleutian arc. Journal of Petrology 25, 88-125.

Deer W.A., Howie R.A., Zussman J., 1992. An introduction to the rock forming minerals. Longman, London, 528 pp.

DeHoog J.C.M., Gall L., Cornell D.H., 2010. Trace element geochemistry of mantle olivine and application to mantle petrogenesis and geothermobarometry. Chemical Geology 270, 196-215.

Desmarais N.R., 1981. Metamorphosed Precambrian ultramafic rocks in the Ruby Range, Montana. Precambrian Research 16, 67-101.

Dick H.J.B. and Bullen T., 1984. Chromian spinel as a petrogenetic indicator in abyssal and alpine-type peridotites and spatially associated lavas. Contributions to Mineralogy and Petrology 86, 54-76.

Dilek Y. and Newcomb S., 2003. Ophiolite concept and the evolution of geological thought. Geological Society of London, Special Paper 373, 504 pp.

Dymek R.F., Brothers S.C., Schiffries C.M., 1988. Petrogenesis of ultramafic metamorphic rocks from the 3800 Ma Isua supracrustal belt, West Greenland. Journal of Petrology 29, 1353-1397.

Evans B.W. and Frost B.R., 1975. Chrome-spinel in progressive metamorphism: a preliminary analysis. Geochimica et Cosmochimica Acta 39, 959-972.

Evans B.W., 1977. Metamorphism of Alpine peridotite and serpentinite. Annual Review of Earth and Planetary Sciences 7, 397-447.

Frost B.R., 1975. Contact metamorphism of serpentinite, chloritic blackwall and rodingite at Paddy-Go-Easy Pass, central Cascades, Washington. Journal of Petrology 16, 272-313.

Fujimaki H. and Yomogida K., 1986a. Petrology of Hayachine ultramafic complex in contact aureole, NE Japan (1). Primary and metamorphic minerals. The Journal of the Japanese Association of Mineralogists, Petrologists and Economic Geologists 81, 1-11.

Fujimaki H. and Yomogida K., 1986b. Petrology of Hayachine ultramafic complex in contact aureole, NE Japan. (II) Metamorphism and origin of the complex. The Journal of the Japanese Association of Mineralogists, Petrologists and Economic Geologists 81, 59-66.

Gervilla F., Padron-Navarta J., Kerestedjian T., Sergeeva I., Gonzalez-Jimenez J., Fanlo I., 2012. Formation of ferrian chromite in podiform chromitites from the Golyamo Kamenyane serpentinite, Eastern Rhodopes, SE Bulgaria: A two-stage process. Contributions to Mineralogy and Petrology 164, 1-15.

Giacobbe C., Viani A., Gualtieri A.F., 2012. High temperature reactions of serpentine group minerals. European Mineralogical Conference, 1, EMC2012-93.

Grieco G. and Merlini A., 2012. Chromite alteration processes within Vourinos ophiolite. International Journal of Earth Sciences 101, 1523-1533.

Gualtieri A.F., Giacobbe C., Viti C., 2012. The dehydroxylation of serpentine group minerals. American Mineralogist 97, 666-680.

Guotana J.M., Morishita T., Yamaguchi R., Nishio I., Tamura A., Tani K., Harigane Y., Szilas K., Pearson D.G., 2018. Contrasting textural and chemical signatures of chromitites in the Mesoarchaean Ulamertoq peridotite body, Southern west Greenland. Geosciences 8, 328.

Haggerty S.E., 1988. Upper mantle opaque mineral stratigraphy and the genesis of metasomatites and alkali-rich melt. Journal of Geological Society of Australia, Special Publication 14, 687-699.

Hajialioghli R. and Moazzen M., 2014. Supra-subduction and mid-ocean ridge peridotites from the Piranshahr area, NW Iran. Journal of Geodynamics 81, 41-55.

Hey M.H., 1954. A new review of the chlorites. Mineralogical Magazine 30, 277-292.

Johnson K.T.M. and Dick H.J.B., 1992. Open system melting and temporal and spatial variation of peridotite and basal at the Atlantis II fracture zone. Journal of Geophysical Research 97, 9219-9241.

Juteau T. and Maury R., 1999. The oceanic crust, from Accretion to Mantle Recycling. Springer-Praxis Series in Geophysics, Heidelberg, Germany, 390 pp.

Kamenetsky V.S., Crawford A.J., Meffre S., 2001. Factors controlling chemistry of magmatic spinel: an empirical study of associated olivine, Cr-spinel and melt inclusions from primitive rocks. Journal of Petrology 42, 655-671.

Kepezhinskas P.K., Defant M.J., Drummond M.S., 1995. Na metasomatism in the island - arc mantle by slab melt - peridotite interaction: Evidence from mantle xenoliths in the

north Kamchatka arc. Journal of Petrology 36, 1505-1527.
Khalili K., Torabi G., Arai S., 2016. Metamorphism of peridotites from Posht-e-Badam Paleozoic ophiolite (Yazd Province, Central Iran). Neues Jahrbuch fur Geologie und Palaontologie-Abhandlungen 280, 59-77.
Khedr M.Z. and Arai S., 2012. Petrology and geochemistry of prograde deserpentinized peridotites from Happo-O'ne, Japan: evidence of element mobility during deserpentinization. Journal of Asian Earth Sciences 43, 150-163.
Khedr M.Z. and Arai S., 2017. Peridotite-chromitite complexes in the Eastern Desert of Egypt: Insight into Neoproterozoic sub-arc mantle processes. Gondwana Research 52, 59-79.
Leake B.E., 1965. The relationship between composition of calciferous amphibole and grade of metamorphism. In: Controls of Metamorphism. (Eds.): W.S. Pitcher, and G.W. Flinn, John Wiley, New York (USA), 299-318.
Leake B.E., Woolley A.R., Arps C.E.S., Birch W.D., Gilbert M.C., Grice J.D., Hawthorne F.C., Kato A., Kisch H.J., Krivovichev V.G., Linthout K., Laird J., Mandarino J., Maresch W.V., Nickel E.H., Rock N.M.S., Schumacher J.C., Smith D.C., Stephenson N.C.N., Ungaretti L., Whittaker E.J.W., Youzhi G., 1997. Nomenclature of amphiboles, report of the subcommittee on amphiboles of the international mineralogical association commission on new minerals and mineral names. European Journal of Mineralogy 9, 623-651.
Mahdavi F., Khakzad A., Nezafati N., Vousughi Abedini M., 2015. Geochemical characteristics of the Kal-e-Kafi Cu-Mo-Au porphyry deposit, Central Iran. Arabian Journal of Geosciences 8, 10739-10758.
Mancini F., Marshall B., Papunen H., 1996. Petrography and metamorphism of the Saaksjarvi ultramafic body, Southwest Finland. Mineralogy and Petrology 56, 185-208.
McDonough W.F. and Sun S.S., 1995. The composition of the Earth. Chemical Geology 120, 223-253.
Melcher F., Meisel T., Puhl J., Koller F., 2002. Petrogenesis and geotectonic setting of ultramafic rocks in the Eastern Alps: constraints from geochemistry. Lithos 65, 69-112.
Mellini M., Rumori C., Viti C., 2005. Hydrothermally reset magmatic spinels in retrograde serpentinites, formation of "ferritchromit" rims and chlorite aureoles. Contributions to Mineralogy and Petrology 149, 266-275.
Merlini A., Grieco G., Diella V., 2009. Ferritchromite and chromian-chlorite formation in mélange-hosted Kalkan chromitite (Southern Urals, Russia). American Mineralogist 94, 1459-1467.
Nazari G., Torabi G., Arai S., Morishita T., 2019. Lower Oligocene calc-alkaline spessartitic lamprophyres from Central Iran (East of Anarak area); an evidence from the Eastern branch of Neotethys subduction-related mantle enrichment. Geotectonics 53, 786-805.
Nosouhian N., Torabi G., Arai S., 2019. Petrological aspects of the Bayazeh Paleozoic ophiolite (Central Iran); implications for Paleo-Tethys subduction. Periodico di Mineralogia 88, 155-184.
Nozaka T., 2003. Compositional heterogeneity of olivine in thermally metamorphosed serpentinite from Southwest Japan. American Mineralogist 88, 1377-1384.
Nozaka T., 2005. Metamorphic history of serpentinite mylonites from the Happo ultramafic complex, central Japan. Journal of Metamorphic Geology 23, 711-723.
Nozaka T., 2010. A note on compositional variation of olivine and pyroxene in thermally metamorphosed ultramafic complexes from SW Japan. The Journal of the Japanese Association of Mineralogists, Petrologists and Economic Geologists 17, 1-5.
Nozaka T. 2011. Constraints on anthophyllite formation in thermally metamorphosed peridotites from southwestern Japan. Journal of Metamorphic Geology 29, 385-398.
Nozaka T., 2018. Compositional variation of olivine related to high-temperature serpentinization of peridotites: Evidence from the Oeyama ophiolite. The Journal of the Japanese Association of Mineralogists, Petrologists and Economic Geologists 113, 219-231.
Nozaka T. and Shibata T., 1995. Mineral paragenesis in thermally metamorphosed serpentinites, Ohsa-yama, Okayama Prefecture. Earth Science Reports, Okayama University 2, 1-12.
Oliver R.L., Nesbitt R.W., Hausen D.M., Franzen N., 1972. Metamorphic olivine in ultramafic rocks from Western Australia. Contributions to Mineralogy and Petrology 36, 335-342.
Paktunc A.D., 1984. Metamorphism of the ultramafic rocks of the Thompson Mine, Thompson nickel belt, northern Manitoba. The Canadian Mineralogist 22, 77-91.
Parkinson I.J. and Pearce J.A., 1998. Peridotites of the Izu-Bonin-Mariana forearc (ODP Leg 125) evidence for mantle melting and melt-mantle interactions in a suprasubduction zone setting. Journal of Petrology 39, 1577-1618.
Pawley A.R., 1998. The reaction talc + forsterite = enstatite + H_2O: New experimental results and petrological implication. American Mineralogist 83, 51-57.
Pearce J.A., Barker P.F., Edwards S.J., Parkinson I.J., Leat P.T., 2000. Geochemistry and tectonic significance of peridotites from the South Sandwich arc basin system, south Atlantic. Contributions to Mineralogy and Petrology 139, 36-53.
Pinsext R.H. and Hirst D.M., 1977. The metamorphism of the Blue River ultramafic body, Cassiar, British Columbia, Canada. Journal of Petrology 18, 567-594.
Ranjbar S., Tabatabaei Manesh S.M., Mackizadeh M.A., Tabatabaei S.H., Parfenova O.V., 2016. Geochemistry of major and rare earth elements in garnet of the Kal-e-Kafi skarn, Anarak Area, Central Iran: Constraints on processes in a hydrothermal system. Geochemistry International 54, 423-438.
Romanko E., Kokorin Yu., Krivyakin B., Susov M., Morozov L., Sharkovski M., 1984. Outline of metallogeny of Anarak area (Central Iran). Geological Survey of Iran, Report TE/No.

21, 136 pp.
Salim H., 2019. Mineralogical characteristics of plagioclase and clinopyroxene in the gabbros and anorthosites from the Kal-e-Kafi intrusion (Northeast of Anarak, Isfahan province, Central Iran). M.Sc. Thesis, University of Isfahan, Isfahan, Iran (in Persian), 150 pp.
Salim H., Torabi G., Nosouhian N., Morishita T., 2018. Mineralogical characteristics of gabbros and anorthosites from the Kal-e-Kafi intrusion (NE of Anarak, Isfahan Province, Iran). Goldschmidt Conference Abstracts, Boston, USA.
Sanford R.F., 1982. Growth of ultramafic reaction zones in greenschist to amphibolite facies metamorphism. American Journal of Science 282, 543-616.
Schwartz S., Guillot S., Reynard B., Lafay R., Debret B., Nicollet C., Lanari P., Auzende A.L., 2013. Pressure-temperature estimates of the lizardite/antigorite transition in high pressure serpentinites. Lithos 178, 197-210.
Scotford D.M. and Williams J.R., 1983. Petrology and geochemistry of metamorphosed ultramafic bodies in a portion of the Blue Ridge of North Carolina and Virginia. American Mineralogist 68, 78-94.
Seyler M., Lorand J.P., Dick H.J.B., Drouin M., 2007. Pervasive melt percolation reactions in ultra-depleted refractory harzburgites at the Mid Atlantic Ridge. - 15°20’N: ODP Hole 1274A. Contributions to Mineralogy and Petrology 153, 303-319.
Shafaii Moghadam, H. and Stern, B., 2014. Ophiolites of Iran: Keys to understanding the tectonic evolution of SW Asia: I) Paleozoic ophiolites. Journal of Asian Earth Sciences 91, 19-38.
Sharkovski M., Susov M., Krivyakin B., Morozov L., Kiristaev V., Romanko E., 1984. Geology of the Anarak area (Central Iran). Geological Survey of Iran, V/O “Technoexport”, Report TE/No, 19, 143 pp.
Shirdashtzadeh N., Torabi G., Meisel T.C., Arai S., Bokhari S.N.H., Samadi R., Gazel E., 2014. Origin and evolution of metamorphosed mantle peridotites of Darreh Deh (Nain Ophiolite, Central Iran): Implications for the Eastern Neo-Tethys evolution. Neues Jahrbuch für Geologie und Palaontologie - Abhandlungen 273, 89- 120.
Spear F.S., 1995. Metamorphic Phase Equilibria and Pressure-Temperature-Time Paths. Mineralogical Society of America, Monograph, Washington, 799 pp.
Springer R.K., 1974. Contact metamorphosed ultramafic rocks in the western Sierra Nevada foothills. California. Journal of Petrology 15, 160-195.
Stocklin J., 1968. Structural history and tectonics of Iran: a review. American Association of Petroleum Geologists Bulletin 52, 1229-1258.
Sun S.S. and McDonough W.F., 1989. Chemical and isotopic systematics of oceanic basalts: implications for mantle composition and processes. In: Magmatism in the Ocean Basins. (Eds.): A.D. Saunders and M.J. Norry, Geological Society of London, Special Publication, 42, 313-345.
Torabi G., 2011. Late Permian blueschist from Anarak ophiolite (Central Iran, Isfahan province), a mark of multi-suture closure of the Paleo-Tethys ocean. Revista Mexicana de Ciencias Geológicas 28, 544-554.
Torabi G., Arai S., Koepke J., 2011a. Metamorphosed mantle peridotites from Central Iran (Jandaq area, Isfahan province). Neues Jahrbuch für Geologie und Palaontologie - Abhandlungen 261, 129-150.
Torabi G., Shirdashtzadeh N., Arai S., Koepke J., 2011b. Paleozoic and Mesozoic ophiolites of Central Iran: Study of amphibolites from Naein, Ashin, Jandaq and Posht-e-Badam ophiolites. Neues Jahrbuch für Geologie und Palaontologie - Abhandlungen 262, 227-240.
Torabi G., 2012a. Late Permian post-ophiolitic trondhjemites from Central Iran: a mark of subduction role in growth of Paleozoic continental crust. Island Arc 21, 215-229.
Torabi G., 2012b, Chromitite absence, presence and chemical variation in ophiolites of Central Iran (Naein, Ashin, Anarak and Jandaq). Neues Jahrbuch für Geologie und Palaontologie - Abhandlungen 267, 171-192.
Torabi G., 2013, Central Iran Ophiolites. Jahad Daneshgahi Publication, Isfahan, Iran, 443 pp.
Tracy R.J., Robinson P., Wolff R.A., 1984. Metamorphosed ultramafic rocks in the Bronson Hill Anticlinorium, central Massachusetts. American Journal of Science 284, 530-558.
Trommsdorff V. and Evans B.W., 1980. Titanian hydroxyl-clinohumite: formation and breakdown in antigorite rocks (Malenco, Italy). Contributions to Mineralogy and Petrology 72, 229-242.
Veblen D.R. and Ribbe P.H., 1982. Amphiboles: petrology and experimental phase relations. Mineralogical Society of America, Reviews in Mineralogy, 9B, 390 pp.
Warren J.M., 2016. Global variations in abyssal peridotite compositions. Lithos 248-251, 193-219.
Warren J.M. and Shimizu N., 2010. Cryptic variations in abyssal peridotite compositions: Evidence for shallow-level melt infiltration in the oceanic lithosphere. Journal of Petrology 51, 395-423.
Whitney D.L. and Evans B.W., 2010. Abbreviations for names of rock-forming minerals. American Mineralogist 95, 185-187.
Wojtulek P. M., Puziewicz J., Ntaflos Th., 2017. MORB melt metasomatism and deserpentinization in the peridotitic member of Variscan ophiolite: an example of the Braszowice - Brzeźnica serpentinites (SW Poland). Journal of Geosciences 62, 147-164.
Yakovenko V., Chinakov I., Kokorin Y., Krivyakin B., 1981. Report on geological prospecting in Anarak area (Kal-e-Kafi - Khuni locality). Geological Survey of Iran, V/O “Technoexport”, Report No. 13, 293 pp.
Yardley B.W.D., 1989. An introduction to metamorphic petrology. Longman, London, 248 pp.

Zanchi A., Zanchetta S., Berra F., Mattei M., Garzanti E., Molyneux S., Nawab A., Sabouri J., 2009. The EoCimmerian (Late? Triassic) orogeny in North Iran. In: South Caspian to Central Iran Basins. (Eds.): M.F. Brunet, M. Wilmsen, J.W.J. Granath, Geological Society of London, Special Publication 312, 31-55.